Int J Earth Sci (Geol Rundsch) (2012) 101:2125–2150
DOI 10.1007/s00531-012-0780-5

ORIGINAL PAPER

Tectonics of the Middle Triassic intracontinental Xuefengshan Belt, South China: new insights from structural and chronological constraints on the basal décollement zone

Yang Chu · Michel Faure · Wei Lin · Qingchen Wang · Wenbin Ji

Received: 2 December 2011 / Accepted: 11 April 2012 / Published online: 22 May 2012

Abstract In orogenic belts, a basal décollement zone often develops at depth to accommodate the shortening due to folding and thrusting of the sedimentary cover. In the Early Mesozoic intracontinental Xuefengshan Belt of South China, such a décollement zone is exposed in the core of anticlines formed by the emplacement of the late-orogenic granitic plutons. Our detailed, multi-scale structural analysis documents a synmetamorphic ductile deformation. In the basal décollement, the Neoproterozoic pelite and sandstone, and the intruding Early Paleozoic granites were deformed and metamorphosed into mylonites and orthogneiss, respectively. The metamorphic foliation contains a NW–SE stretching lineation associated with top-to-the-NW kinematic indicators. The ductile shearing of these high-strained rocks can be correlated with NW-verging folds and thrusts recognized in the Neoproterozoic to Early Triassic sedimentary cover. Monazite U–Th–Pb_{tot} chemical dating, and zircon SIMS U–Pb dating provide age constraints of the ductile shearing between 243 and 226 Ma, and late-orogenic granite emplacement around 235–215 Ma. In agreement with recent geochronological data, these new results show that the Xuefengshan Belt is an Early Mesozoic orogen dominated by the NW-directed shearing and thrusting. At the southeastern boundary of the Xuefengshan Belt, the Chenzhou-Linwu fault separates the Early Mesozoic domain to the NW from the Early Paleozoic domain to the SE. The tectonic architecture of this belt was possibly originated from the continental underthrusting to the SE of the South China block in response to northwest-directed subduction of the Paleo-Pacific plate.

Keywords Intracontinental belt · Basal décollement zone · Xuefengshan · South China block · Triassic tectonics

Introduction

Because of their considerable distance, 1,000 km or more, from convergent plate boundaries, intracontinental orogens remain an enigmatic tectonic feature for geologists. Some examples of intracontinental belts are documented in the Miocene Tianshan orogen in Central Asia (Molnar and Tapponnier 1975; Tapponnier and Molnar 1979; Hendrix et al. 1992; Avouac et al. 1993), the Cenozoic Laramide orogen in North America (Dickinson and Snyder 1978; English and Johnston 2004), the Cenozoic Pyrenees in Europe (Roure et al. 1989; Choukroune 1992; Sibuet et al. 2004), the Early Paleozoic South China belt (Faure et al. 2009; Charvet et al. 2010; Li et al. 2010b), and the Neoproterozoic Petermann and Paleozoic Alice Springs orogens in Central Australia (Hand and Sandiford 1999; Sandiford et al. 2001; Raimondo et al. 2010). These intracontinental orogens are characterized by fold-and-thrust

Electronic supplementary material The online version of this article (doi:10.1007/s00531-012-0780-5) contains supplementary material, which is available to authorized users.

Y. Chu · M. Faure · W. Lin (✉) · Q. Wang · W. Ji
State Key Laboratory of Lithopheric Evolution, Institute of Geology and Geophysics, Chinese Academy of Sciences, 19 Beitucheng Western Road, Chaoyang District, Beijing 100029, People's Republic of China
e-mail: linwei@mail.iggcas.ac.cn

Y. Chu · M. Faure
Institut des Sciences de la Terre d'Orléans, Campus Géosciences, Université d'Orléans, 1A, Rue de la Férollerie, 45071 Orléans Cedex 2, France

Y. Chu · W. Ji
Graduate University of Chinese Academy of Sciences, Beijing 100049, China

belts, regional décollement zones, absence of ophiolitic suture, absence of subduction complex and magmatic arc, and limited or even absent crustal melting and metamorphism.

In central South China, the Xuefengshan Belt (XFSB) exposes well-preserved structures indicating an intracontinental orogeny of Triassic age. The XFSB plays an important role in understanding of the tectonic pattern of the South China block; however, its architecture and geodynamics remain poorly understood (Qiu et al. 1998, 1999; Yan et al. 2003; Wang et al. 2005). Despite of significant compressional deformation in the subsurface sedimentary strata, no highly metamorphosed basement rocks are exposed, suggesting the existence of a décollement zone that would accommodate the deformation at depth. Although décollement zones are also present in the outer zones of many collisional orogens, such as the Alps (Escher and Beaumont 1997), or the Zagros (McQuarrie 2004), little attention has been paid to basal décollement zones in intracontinental belts. The décollement zone well exposed in the XFSB makes this intracontinental orogen a good example to investigate this major structure. In order to better document the structural features of an intracontinental orogen, this paper presents detailed field and microscope scale structural analyses of the ductile décollement zone in the XFSB. To better constrain the timing of the deformation, new monazite U–Th–Pb_{tot} chemical dating of the syn-kinematic metamorphism coeval with the formation of the ductile décollement zone is presented. In addition, zircon U–Pb dating and monazite dating of the late-orogenic granites that post-date the deformation are also performed.

Geological setting of the South China block (SCB)

The SCB formed in the Neoproterozoic, around 900 Ma, due to the collision between the Yangtze and the Cathaysia blocks, which were amalgamated during the Jiangnan orogeny. In the eastern part of this belt, the Jiangshan-Shaoxing Fault represents the ophiolitic suture of the Neoproterozoic collision (Charvet et al. 1996; Li 1999; Li et al. 2009; Fig. 1a), but its southwestern extension is not well established due to poor exposure. From the Late Neoproterozoic to Middle Silurian, ca. 10-km-thick continuous terrigenous sedimentation took place in the southern part of the SCB. In the northern part of the SCB, the Cambrian-Ordovician sedimentation is characterized by black shale and limestone, followed by the deposition of a thick Silurian turbidite formation (Wang and Li 2003; BGMRJX 1984; BGMRHN 1988). From the Late Ordovician, (ca. 450 Ma) to Silurian, an intracontinental orogeny that partly reworked the Jiangshan-Shaoxing suture occurred in the southeastern part of the SCB. This orogen was characterized by ductile deformation, intermediate pressure-intermediate temperature metamorphism, crustal melting at approximately 440–430 Ma, and emplacement of post-orogenic plutons from 430 to 400 Ma. A regional Middle Devonian unconformity indicates the end of deformation (Wang et al. 2007b; Faure et al. 2009; Wan et al. 2009; Li et al. 2010b; Charvet et al. 2010).

The Early Mesozoic is the most important period for the tectonics of the SCB. To the north, the SCB subducted beneath the North China block, forming the southern part of the Qinling-Dabie Belt, which is also an intracontinental belt developed after the Ordovician collision between the North China and the South China blocks (e.g., Mattauer et al. 1985; Hacker and Wang 1995; Faure et al. 1999, 2008). To the southwest, the over 1,000-km-long Jinshajiang-Song Ma suture extends from western Yunnan to North Vietnam. This major belt is likely related to the collision between the SCB and the Indochina block (Lepvrier et al. 1997, 2004, 2008, 2011; Wang et al. 2000; Carter et al. 2001; Wallis et al. 2003; Harrowfield and Wilson 2005; Carter and Clift 2008; Roger et al. 2008, 2010; Chen et al. 2011). A Triassic deformation also exists by places to the east of the study region in the Cathaysia block (Fig. 1a), as documented by a Late Triassic unconformity, and locally by ca. 250–225 Ma magmatism (BGMRJX 1984; BGMRFJ 1985; BGMRZJ 1989; Faure et al. 1996; Chen 1999; Xiao and He 2005). Furthermore, in the central part of the SCB, the deformation pattern, characterized by NE–SW to NNE–SSW trending folds and faults with an overall northwest vergence, forms the XFSB (Fig. 1a).

Architecture of the Xuefengshan Belt

The age and structures of the XFSB are still controversial. Some authors argue for an Early Paleozoic age (Qiu et al. 1998, 1999), but others propose a Cretaceous one (Yan et al. 2003). Recent studies suggest that the XFSB developed in the Middle Triassic, since Early Triassic rocks are folded, but Late Triassic to Early Jurassic terrigenous rocks, represented by red sandstone, conglomerate, and mudstone unconformably overly the deformed series (BGMRHN 1988; Wang et al. 2005; Chu et al. 2011).

Unlike the southern areas of the SCB, the XFSB exposes a weak Early Paleozoic deformation, as indicated by a low angle (not higher than $\sim 20°$) unconformity between Devonian and pre-Devonian rocks, and the consistency of cleavage development in all the sedimentary series ranging from Late Neoproterozoic to Early Triassic (BGMRHN 1988; Chu 2012). Thus, in the XFSB, the main tectonic event appears to develop after the Early Paleozoic.

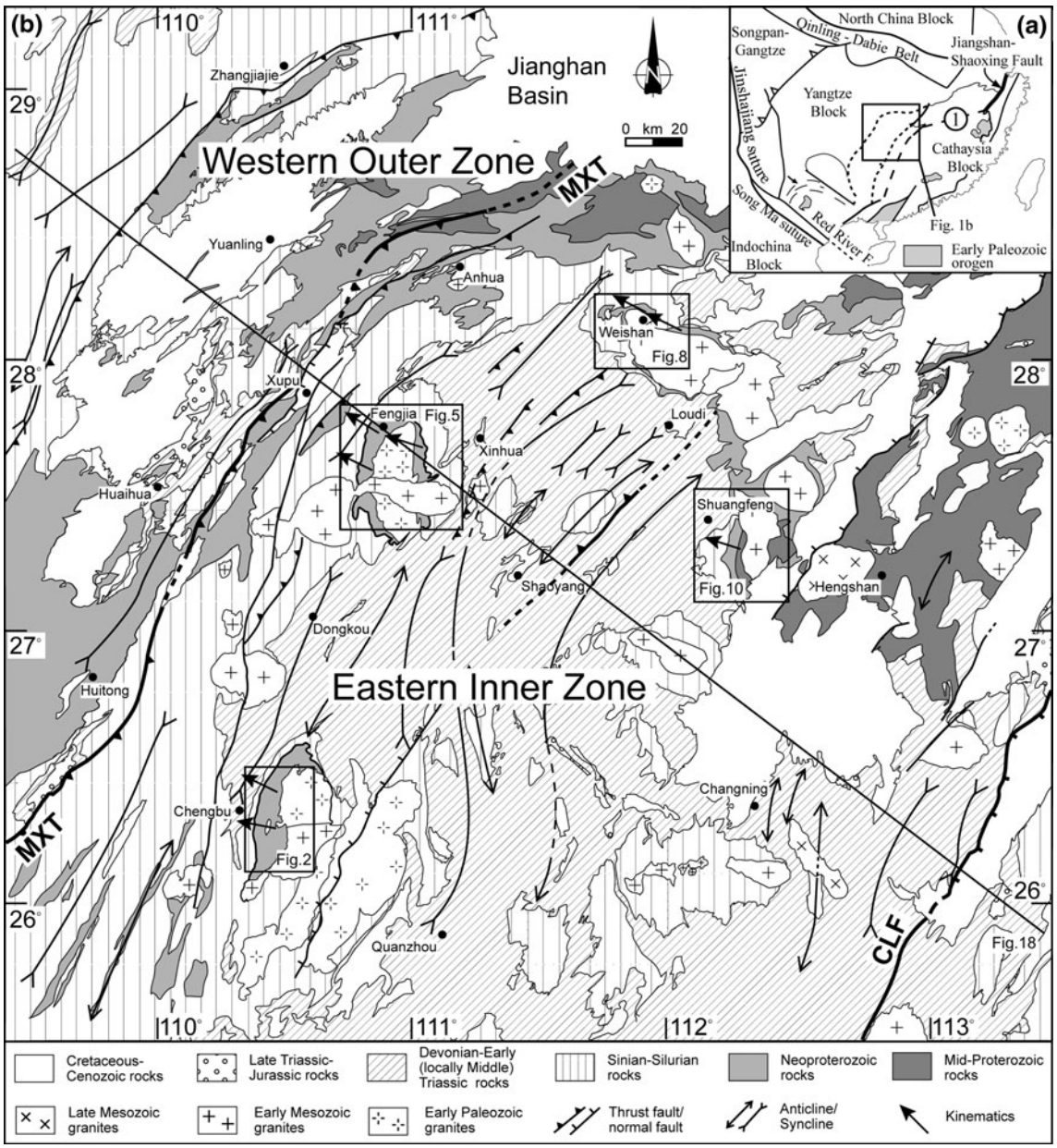

Fig. 1 **a** Tectonic map of the South China block with the location of the study area (modified after Faure et al. 2009; Chu 2012). *1* Southwestern extension of the Jiangshan-Shaoxing Fault. **b** Structural map of the Xuefengshan Belt (modified after 1:500,000 Geological map of Hunan, BGMRHN 1988). *MXT* the main Xuefengshan thrust, *CLF* Chenzhou-Linwu fault (extension of the Jiangshan-Shaoxing fault)

The XFSB is divided into two zones: the Western Outer Zone and the Eastern Inner Zone, separated by the Main Xuefengshan Thrust, along which metamorphic rocks of the Eastern Inner Zone are thrust onto the sedimentary rocks of the Western Outer Zone (Chu et al. 2011; Fig. 1b). This thrust represents also the cleavage front in the belt. West of the Main Xuefengshan Thrust, ductile deformation is weak and penetrative cleavage is absent. The ductile deformation is restricted to the Eastern Inner Zone. Three stages of deformation, namely D_1, D_2, D_3, have been recognized in the Neoproterozoic to Early Triassic sedimentary series that form the Eastern Inner Zone (Chu 2012). The D_1 structures are characterized by NW-verging folds and thrusts often associated with a SE dipping, axial planar, slaty cleavage (S_1), and a NW–SE mineral and stretching lineation, represented by elongated clasts in terrigenous rocks, quartz pressure shadows around pyrite in slates, and sericite or chlorite fibers. Kinematic indicators such as asymmetric pressure shadows or shear bands show a top-to-the-NW shearing that agrees with fold vergence.

The D_1 structures are subsequently reworked by SE-directed folds and thrusts attributed to a D_2 event. A NW-dipping fracture, or slaty cleavage (S_2), develops in the axial planes of D_2 folds, but the stretching lineation is rare. Lastly, upright folds associated with a vertical cleavage (S_3) and a vertical stretching lineation formed during the D_3 phase. The XFSB experienced a lower greenschist facies metamorphism developed during D_1 (Chu et al. 2011).

Plutonic rocks are widespread in the XFSB (Fig. 1b). On the basis of their ages, lithology, and deformation, these granitic rocks can be divided into an Early Paleozoic group and a Triassic group. The Early Paleozoic plutons (ca. 430–410 Ma) underwent a ductile deformation during the Middle Triassic, whereas the undeformed Late Triassic granites intruded the deformed pre-Mesozoic series. The Triassic granitic plutons that occupy an area of more than 5,600 km^2 consist of two-mica granite, biotite monzonite, two-mica monzonite, and biotite-hornblende granite with lesser amounts of granodiorite and tourmaline granite (BGMRHN 1988; Wang et al. 2007a). Previous geochemical studies show that these peraluminous granitic magmas are formed by crustal melting after the Early Triassic compression (Chen et al. 2006, 2007a, b; Wang et al. 2007a).

In the litho-stratigraphic series of the XFSB, the Late Neoproterozoic (Sinian) pelite and graphitic layers, Cambrian black shale, as well as Devonian, Carboniferous, Permian, and Early Triassic pelitic layers, including some coal measures, played an important role in the structural evolution of the XFSB (Yan et al. 2003). These soft layers with a low yield stress acted as décollement levels that accommodated a major part of the regional shortening during Triassic folding and thrusting.

The deepest layer of the Xuefengshan series is represented by micaschist and schistose siltstones of Neoproterozoic (pre-Sinian) age. This ductile synmetamorphic zone of 2–5 km in width cropping out due to the structural high formed during the emplacement of Late Triassic granites and was exposed to the surface by subsequent erosion. This litho-tectonic unit represents the main structural discontinuity of the XFSB that separates the sedimentary cover and the basement rocks. In the following, it will be interpreted as the basal décollement zone, whereas the Sinian and Paleozoic pelitic layers are subordinate décollement levels. In the next section, the structural features of this basal décollement zone are presented.

Structural analysis of the basal décollement zone

In the Western Outer Zone of the XFS, the shortening of the sedimentary cover, accommodated by box folding, is estimated to 20 % (Yan et al. 2003). The total amount of crustal shortening experienced by the XFSB, however, is probably underestimated, since in the Eastern Inner Zone, shortening accommodated by ductile mechanisms such as pressure solution, folding, slip on the layers, and the total displacement on brittle thrust faults is not taken into account. As indicated in the previous section, neither significant ductile deformation nor metamorphism is present in the Neoproterozoic to Early Triassic series. In contrast, the pre-Sinian micaschists exhibit a synmetamorphic ductile shearing. Detailed structural investigations were carried out in four representative areas where metamorphic rocks outcrop well (Fig. 1b). In the next sections, we shall describe the mesoscale features, such as the planar and linear fabrics, folds observed in the décollement zone, and the microstructures, including quartz texture, and *c*-axis fabrics.

Chengbu area

East of Chengbu (Figs. 1b, 2a), the Miaoershan granitic massif consists of Early Paleozoic and Early Mesozoic plutons (BGMRHN 1988; Zhou 2007). Mid-Late Proterozoic greenschist facies slate, schistose sandstone, quartzite, and garnet-bearing two-micaschist are exposed in the vicinity of the Miaoershan pluton (Fig. 2a, b). These rocks show a penetrative foliation gently dipping to the NW or SE, a NW–SE mineral and stretching lineation, and a NE–SW crenulation lineation, and microfold axes (Fig. 2c–f). Mylonites and ultramylonites are observed near Lanrong and east of Jiangping (Fig. 2a). This zone that represents the deepest unit of the XFSB in the Chengbu area is characterized by NW-directed structures, which are reworked by upright folds, sometimes with a subvertical crenulation cleavage, and crenulation lineation similar to the D_3 event observed in the sedimentary series.

Mesoscopic deformation

In order to better understand the mechanism of deformation, we outline here the representative macroscopic structures. Above the décollement zone, the Late Neoproterozoic (Sinian) to Paleozoic series is weakly metamorphosed and deformed by NW-verging folds related to the D_1 event. The underlying mylonitic sandstone and mudstone show a pervasive foliation. Numerous quartz lenses distributed in the micaschists argue for important fluid circulation. In outcrop-scale sections that are perpendicular to the foliation and parallel to the lineation, quartz lenses asymmetry indicates a top-to-the-NW sense of shear (Fig. 3a, b). Moreover, the Paleozoic granite is intensely mylonitized with a gneissic structure (Fig. 3c), and some granitic dykes, intruding into the micaschists, yield an

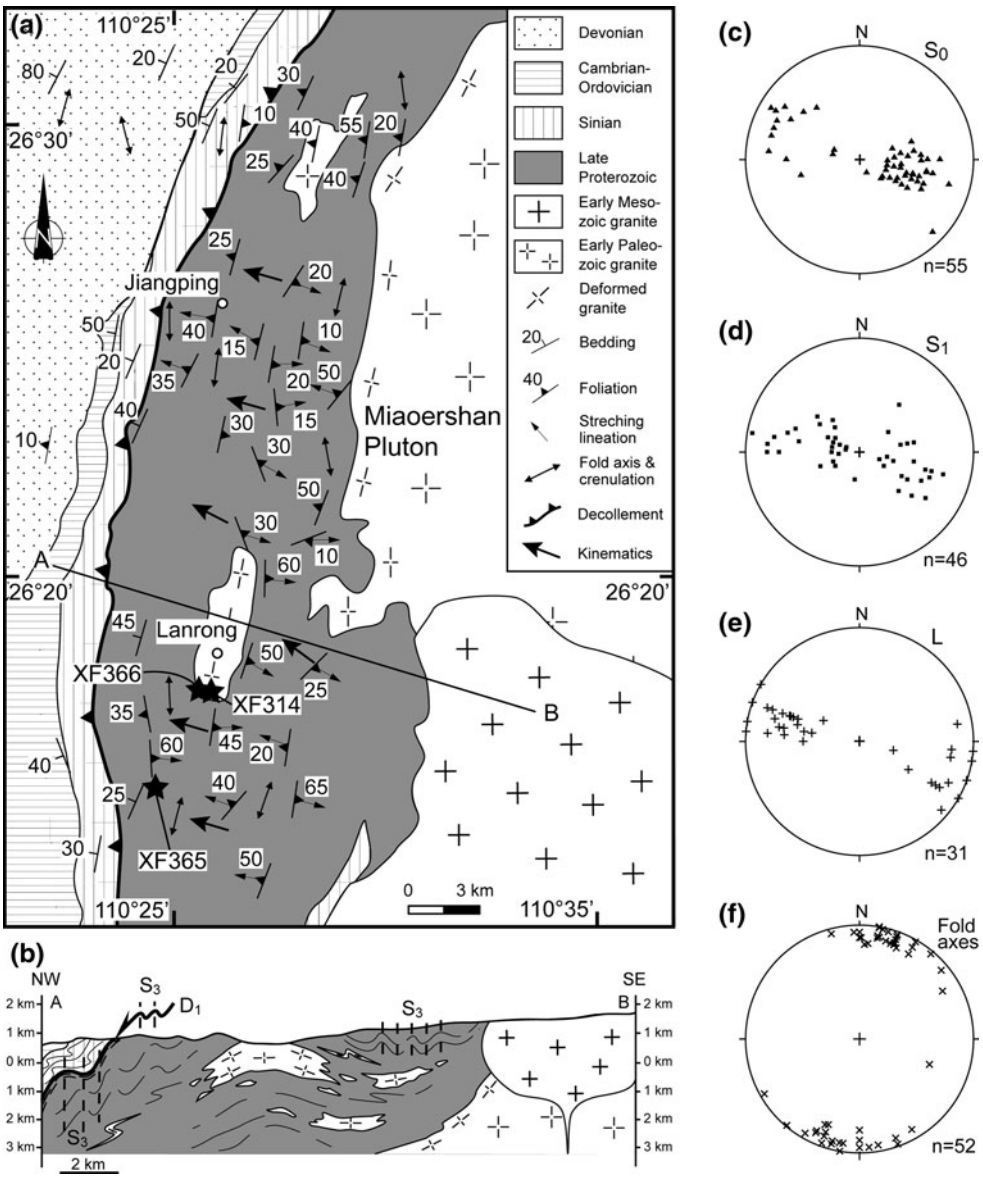

Fig. 2 **a** Detailed geologic map of the basal décollement zone, east of the Chengbu (modified after 1:500,000 Geological map of Hunan, BGMRHN 1988). **b** General cross section of the area. Orientation plots (Schmidt net, lower hemisphere) of the structural elements, **c** bedding, **d** S_1 foliation, **e** stretching lineation, **f** F_3 fold axes and crenulation lineation

asymmetric sigmoidal shape with a top-to-the-NW sense of shear (Fig. 3d). All the above-mentioned structures indicate a post-solidus shearing developed after granite emplacement.

Microfabrics

At the microscopic scale, the shear sense is clearly evidenced by numerous kinematic indicators, such as sigma-type porphyroclast systems, mica fish, and shear bands. In meta-sandstone, quartz clasts are surrounded by chlorite or mica pressure shadows, and the matrix is deformed with shear bands. As indicated by the concentration of phyllosilicates in the foliation planes, pressure shadows around clasts, and dissolution features, pressure solution is the main deformation mechanism in these rocks (Fig. 4a, b). In quartzite, the metamorphic crystallization of white mica and the recystallization of quartz are pervasively developed. East of Jiangping (Fig. 2a), quartzite is deformed into mylonite with sigmoidal mica fish arranged along shear bands, indicating a top-to-the-NW shear sense (Fig. 4c). In micaschist, in spite of the subsequent alteration that changed garnet porphyroblasts into a chlorite–quartz assemblage, the asymmetric quartz pressure shadows indicate also a top-to-the-NW sense of shear (Fig. 4d).

In order to decipher the deformation pattern of the high-strain décollement zone, we investigated the quartz *c*-axis preferred orientation with respect to the texture of the quartz aggregates observed in some mylonitic samples. In the analyzed mylonite, two types of quartz microstructures can be recognized. The first type occurs generally in micaschist. It consists of anhedral or subhedral quartz grains

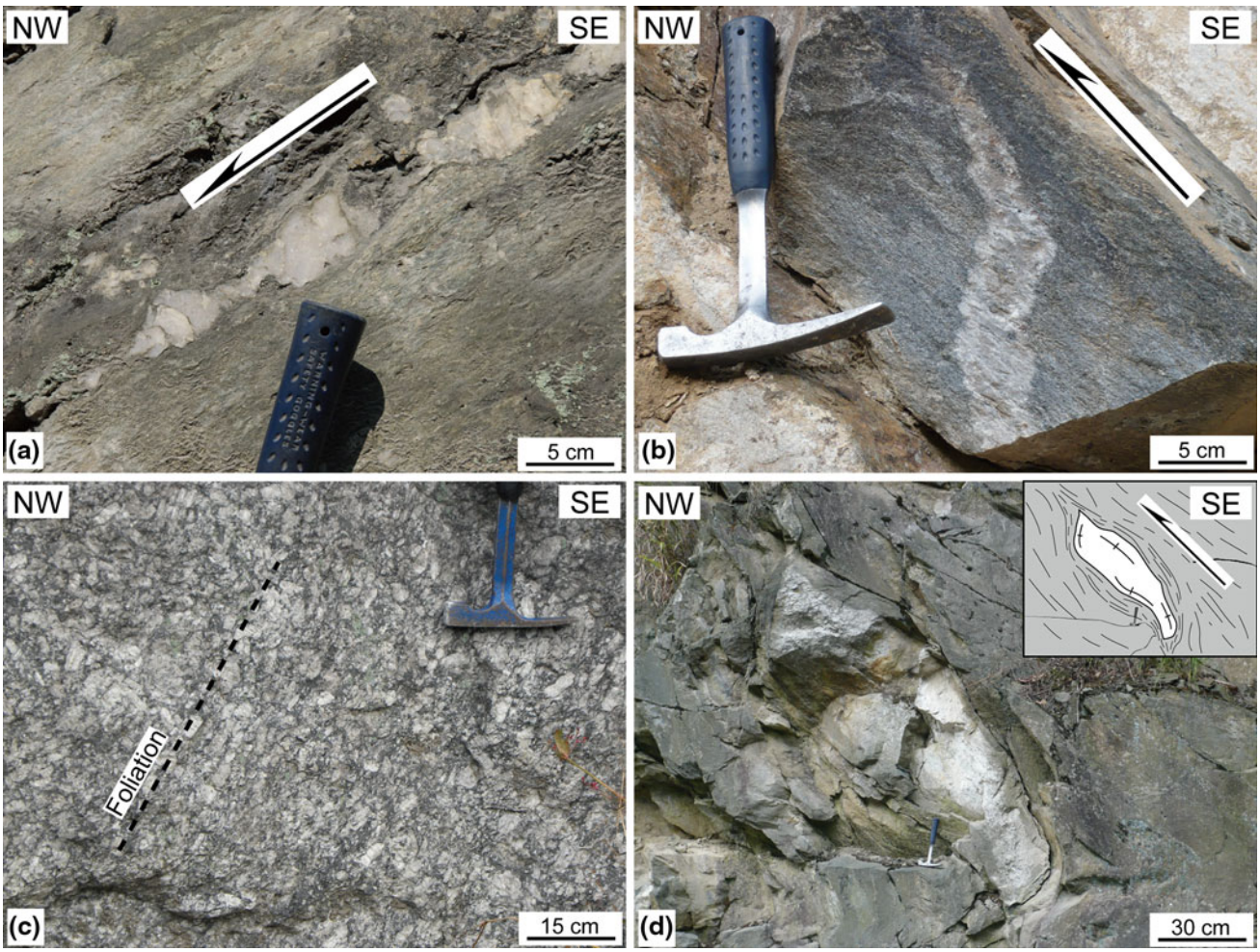

Fig. 3 Examples of structures observed in the basal décollement zone in the Chengbu area. **a** Sigmoidal quartz veins in the mylonitic Neoproterozoic quartzite, east of Jiangping. **b** Sheared vein in micaschist, northeast of Lanrong. **c** Foliated Paleozoic granite, Lanrong. **d** Deformed granitic lense within a micaschist matrix, east of Lanrong

with straight boundaries and platen shape (Fig. 5a). In some cases, the grain boundaries tend to arrange in triple junctions with interfacial angles close to 120°. No obvious dynamic recrystallization is observed. The second one is developed in quartzite or micaceous quartzite. In these rocks, two groups of quartz grains, namely ~1-mm-sized clasts, and ~70 μm grains in matrix, are identified (Fig. 5b). Quartz clasts are generally elongated parallel to the foliation and subdivided into several subgrains with oblique subgrain boundaries. These grains exhibit undulose extinction; along the clast boundaries, newly formed anhedral fine grains are isolated from the host grain by subgrain rotation recrystallization.

Quartz *c*-axis measurements were performed from thin sections cut in the *XZ* plane (i.e., perpendicular to the foliation and parallel to the lineation) with a universal stage from 11 samples in which quartz aggregates belong to one of the two types described above. The *c*-axis patterns can also be grouped into two types, corresponding to the categorization of quartz microstructures. One type consists of crossed girdles with an opening angle of ~75°, and a point maximum close to the Y-axis. Along the girdles, point maxima in the *XZ* plane, and inclined at low angles (less than 45°) to *Z*, are consistent with the dominance of basal $\langle a \rangle$ slip mechanism. *C*-axis concentration around *Y* indicates prism $\langle a \rangle$ slip. This type is observed in samples XF286, XF290, XF296, XF299, XF311, XF312, except that no point maximum around Y-axis is observed in XF286, probably due to a lower temperature (Fig. 6). Another pattern of quartz *c*-axis fabric exhibits maxima close to the *Y*-axis, and a single oblique girdle, pointing to basal, rhomb and prism slip systems active at the same time. Such a pattern corresponds to samples XF300, XF309, XF310, XF315, XF317 (Fig. 6). Both types of quartz *c*-axis patterns indicate that the preferred orientation in the mylonite was developed under low-temperature

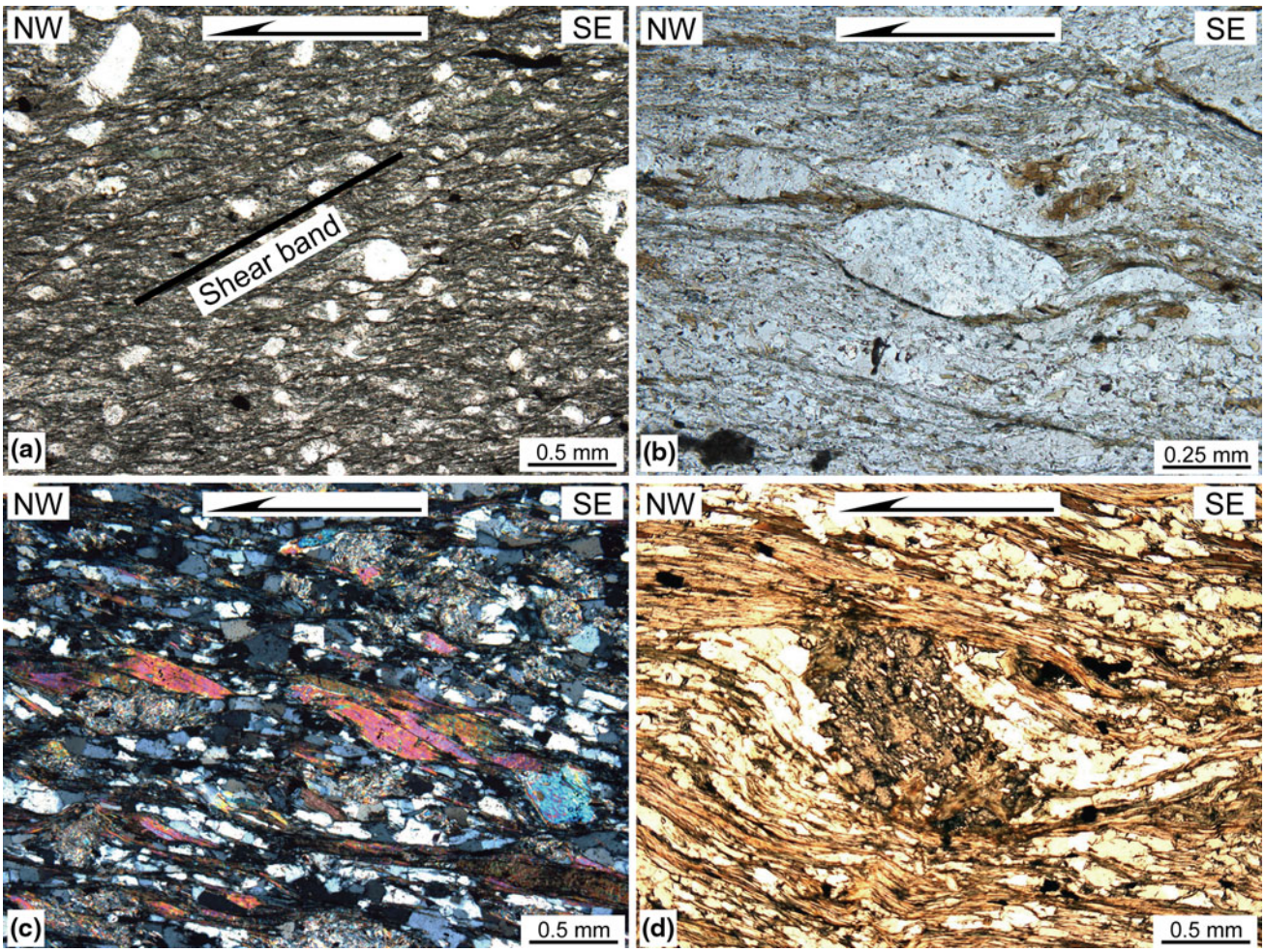

Fig. 4 Microscopic deformational features of the basal décollement zone of the Chengbu area. **a** Sheared Neoproterozoic conglomerate with shear bands and quartz clasts with asymmetric pressure shadows showing a top-to-the-NW sense of shear, west of Lanrong. **b** Sigmoidal feldspar porphyroblast in sandstone with a top-to-the-NW shear sense, east of Jiangping. **c** Garnet porphyroblast with quartz pressure shadows showing the top-to-the-NW sense of shear. **d** Mica fishes in micaschist with a top-to-the-NW shear sense, southeast of Jiangping

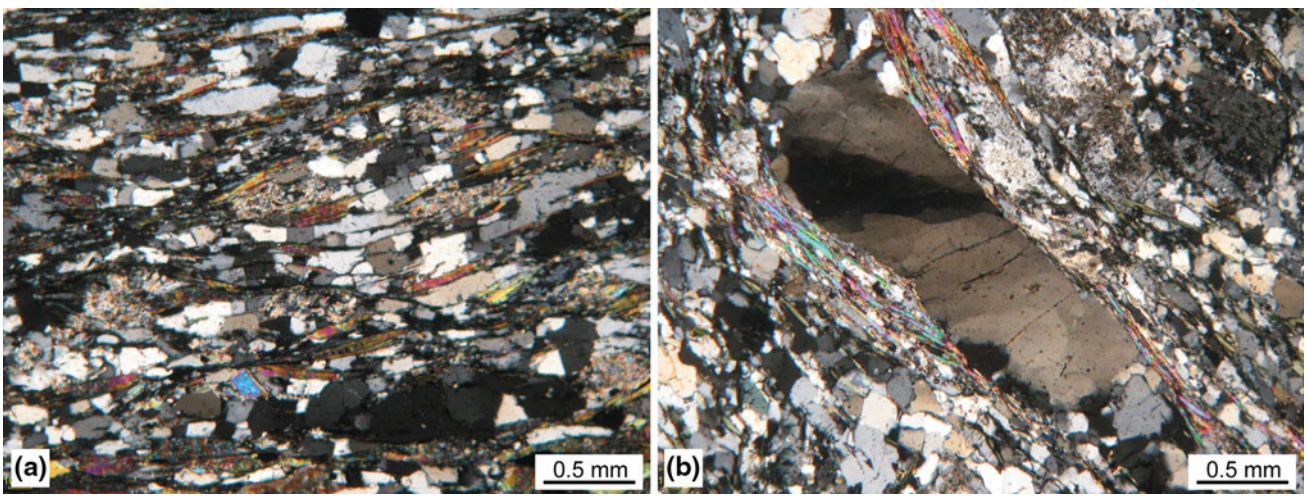

Fig. 5 Microscopic photos showing deformation pattern of quartz grains in the basal décollement in the Chengbu area. **a** Anhedral or subbhedral quartz grains with straight boundaries and platen shape. **b** Quartz clasts elongated parallel to the foliation and subdivided into several subgrains with oblique subgrain boundaries, and undulose extinction

metamorphic conditions, and probably in presence of hydrous material (Passchier and Trouw 2005).

Fengjia-Shuiche area

Lower greenschist facies metamorphic rocks, including meta-sandstone, quartzite, and micaschist, crop out around the Baimashan granite (Figs. 1, 7a). This massif is composed of Paleozoic and Early Mesozoic plutons. The metamorphic rocks are exposed in a ca. 20-km-large anticline, probably due to the emplacement of the Late Triassic plutons. The host rocks are ductilely deformed and overlain by unmetamorphosed Late Neoproterozoic (Sinian) to Paleozoic sedimentary rocks. The foliation of the host rocks dips to the west and east in the western and eastern sides of the anticline, respectively (Fig. 7b–d). The deformed metamorphic rocks are interpreted as products of the basal décollement zone (Fig. 7a, b), in which the intensity of ductile deformation increases downward.

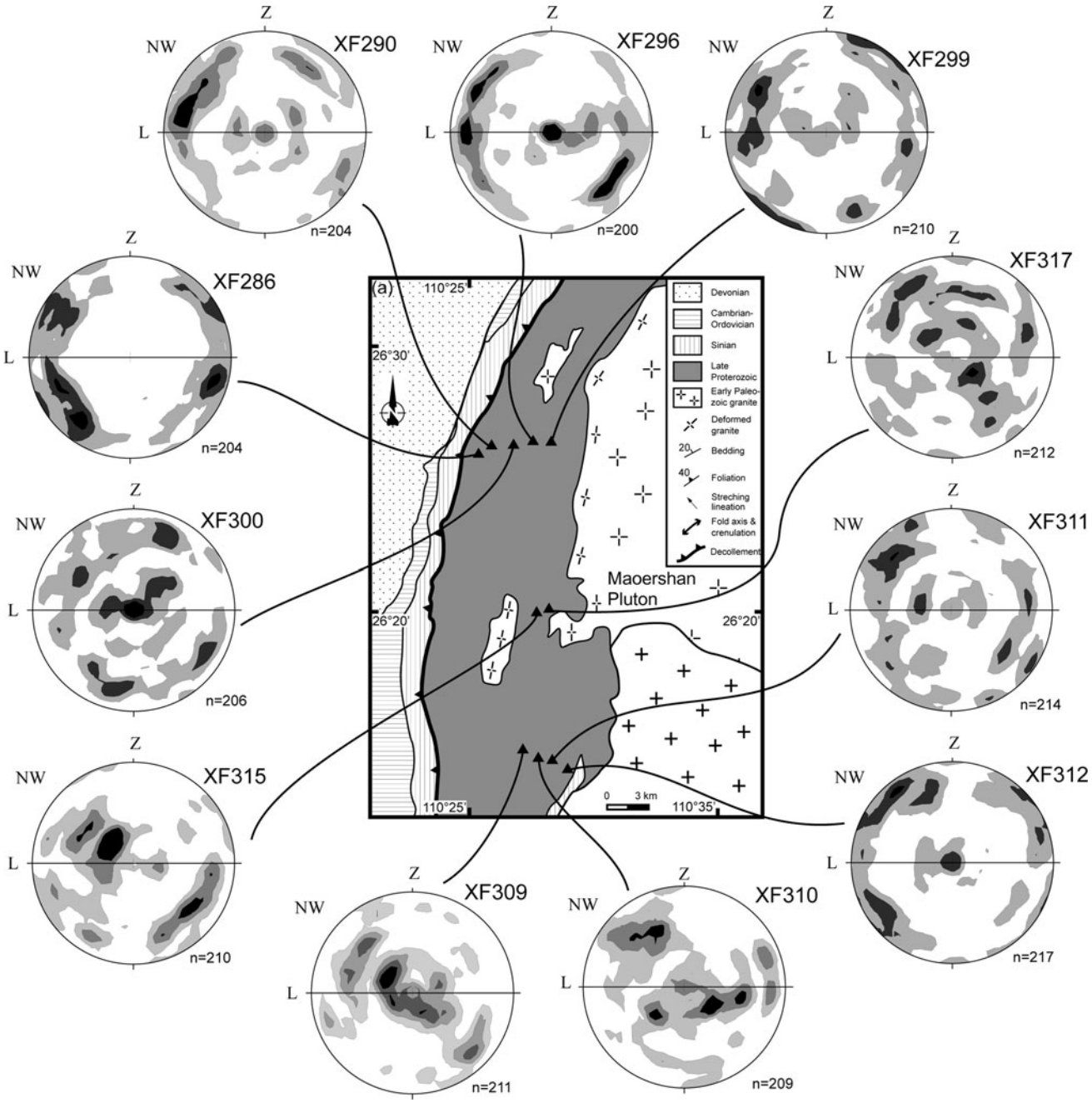

Fig. 6 Quartz *c*-axis preferred orientation (Schmid net, lower hemisphere) for the mylonitic rocks in the basal décollement zone of Chengbu area. Contour intervals are 1 %

Mesoscopic deformation

At the outcrop scale, the metamorphic and deformation style shows some differences between the western and eastern limbs of the anticline.

To the west of Fengjia (Fig. 7a), close to the sedimentary Neoproterozoic–Paleozoic series, in spite of the ductile deformation, the sedimentary structures are still preserved. When moving eastwards, the intensity of deformation and metamorphism increases, and the sedimentary bedding is transposed by a S_1 foliation. Near Fengjia, the S_1 foliation exhibits a flat-lying attitude, but small changes in dip indicate that S_1 is involved in a late upright folding. The NNE–SSW crenulation, centimeter to meter-scale folds and a vertical cleavage are in agreement with this late upright folding event (Fig. 8a). Close to the pluton, S_1 is tilted to subvertical and deformed by centimeter- to meter-scale NE–SW trending fold axes with subhorizontal axial planes, locally associated with a flat-lying foliation represented by the preferred orientation of mica flakes. These structures argue for vertical shortening that might be due to the intrusion of the Early Mesozoic granite (Figs. 7b, 8b). Syn-S_1 intrafolial folds are also refolded during this event. Our field observations show that the most pervasively deformed rocks crop out in the lowermost part of the series where biotite appears.

South of Fengjia, near Yanxi (Fig. 7a), a well-pronounced foliation develops in the Neoproterozoic conglomerate in which the pebbles exhibit a N120°E trending preferred orientation consistent with the regional lineation

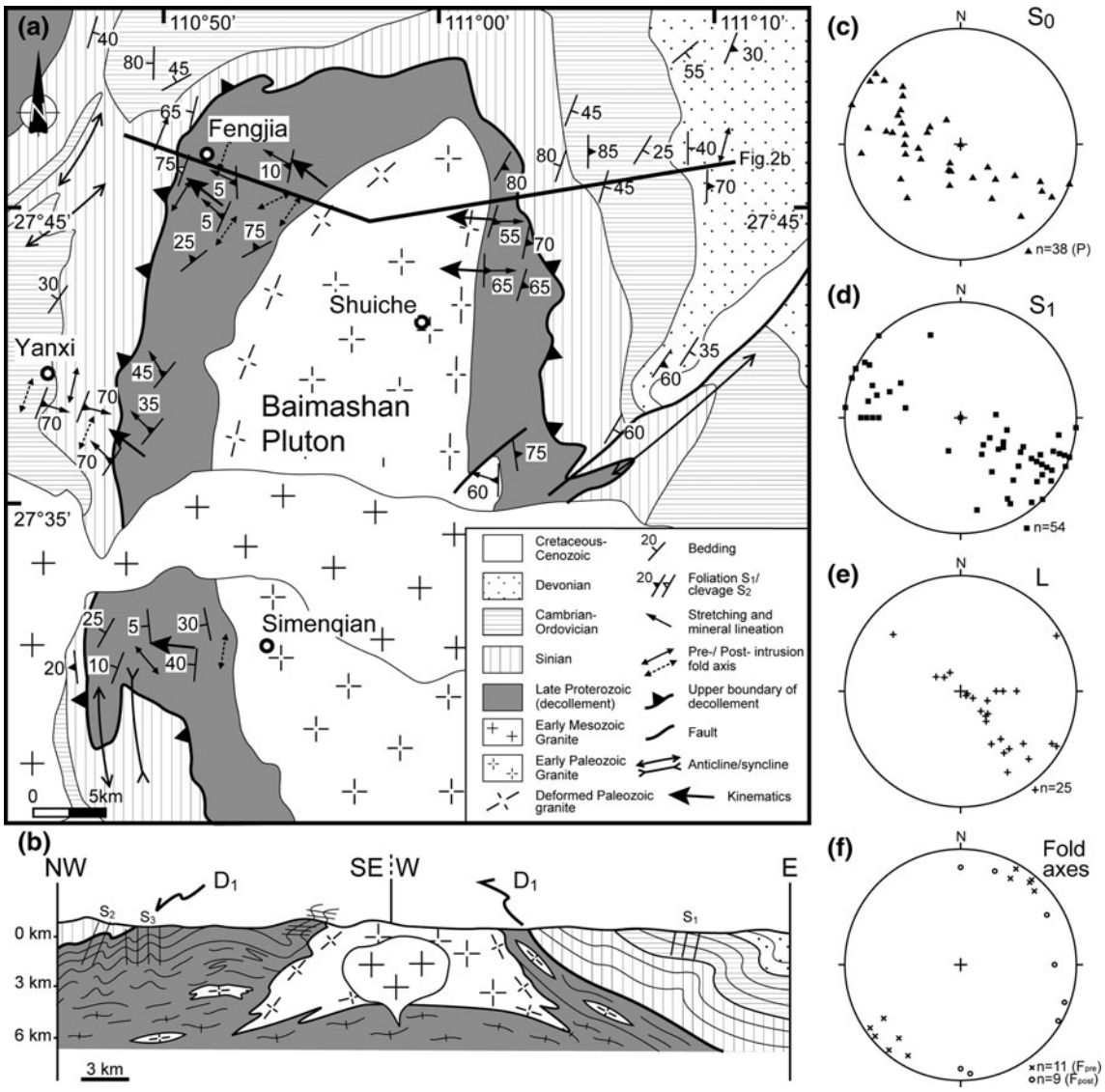

Fig. 7 **a** Detailed geologic map of the Fengjia-Shuiche area (modified after 1:500,000 Geological map of Hunan, BGMRHN 1988). **b** Cross sections of the area. Orientation plots (Schmidt net, lower hemisphere) of the structural elements, **c** bedding, **d** S_1 foliation, **e** stretching lineation, **f** fold axes and crenulation lineation. F_{pre} and F_{post} fold axes before and after the intrusion of the pluton


NW
SE
(a)
0.5 m
NE
SW
Crenulation
Foliation
(b)
0.5 m
N120°
(c)
20 cm
W
E
(d)
20 cm
W
E
(e)
0.5 m
NW
SE
(f)
3 cm
110°
Mineral lineation
(g)
2 cm
(h)
20 cm

◀ **Fig. 8** Photographs illustrating the deformation of the Fengjia-Shuiche area. **a** Upright folds in the high-strain zone, southeast of Fengjia. **b** *Vertical* foliation with a *horizontal* crenulation, southeast of Fengjia. **c** Stretched pebbles trending NW–SE in meta-conglomerate, east of Yanxi. **d** Boudinaged quartz vein in quartzite, west of Simenqian. **e** Meter-scale recumbent fold in quartzite, west of Simenqian. **f** Fractured feldspar clast in Neoproterozoic (Sinian) conglomerate, indicating a top-to-the-NW shear sense, northeast of Shuiche. **g** Mineral lineation due to the reorientation of andalusite crystallized during the contact metamorphism of the Early Paleozoic Baimashan pluton, northeast of Shuiche. **h** Mylonitic Early Paleozoic granite with compositional layering, southeast of Shuiche

observed in the micaschists and meta-sandstones (Figs. 7e, 8c). In the sedimentary cover, the rocks are deformed in accordance with the structure observed in the décollement zone. For instance, a closely spaced cleavage and a NW–SE mineral and stretching lineation marked by elongated mineral aggregates are conspicuous.

More southerly, west of Simenqian, the décollement is represented by a near-horizontal foliation in meta-sandstone and conglomerate with sheared and boudinaged quartz veins (Fig. 8d). Moreover, intra-folial recumbent folds are also observed in weakly metamorphosed sandstone indicating that the original bedding is totally transposed into the S_1 foliation (Fig. 8e).

To the east of the pluton and northeast of Shuiche, meta-conglomerate, meta-pelite, and micaschist that crop out in the décollement are of a higher metamorphic grade than to the west. In the Neoproterozoic meta-conglomerate, the cleavage is represented by a penetrative slaty cleavage, along which variably sized pebbles are oriented and sheared, exhibiting a sigmoidal shape. The cleavage intensity decreases upwards in Sinian and lower Paleozoic rocks, which contain generally a spaced cleavage. Shear sense is indicated by asymmetric pressure shadow around

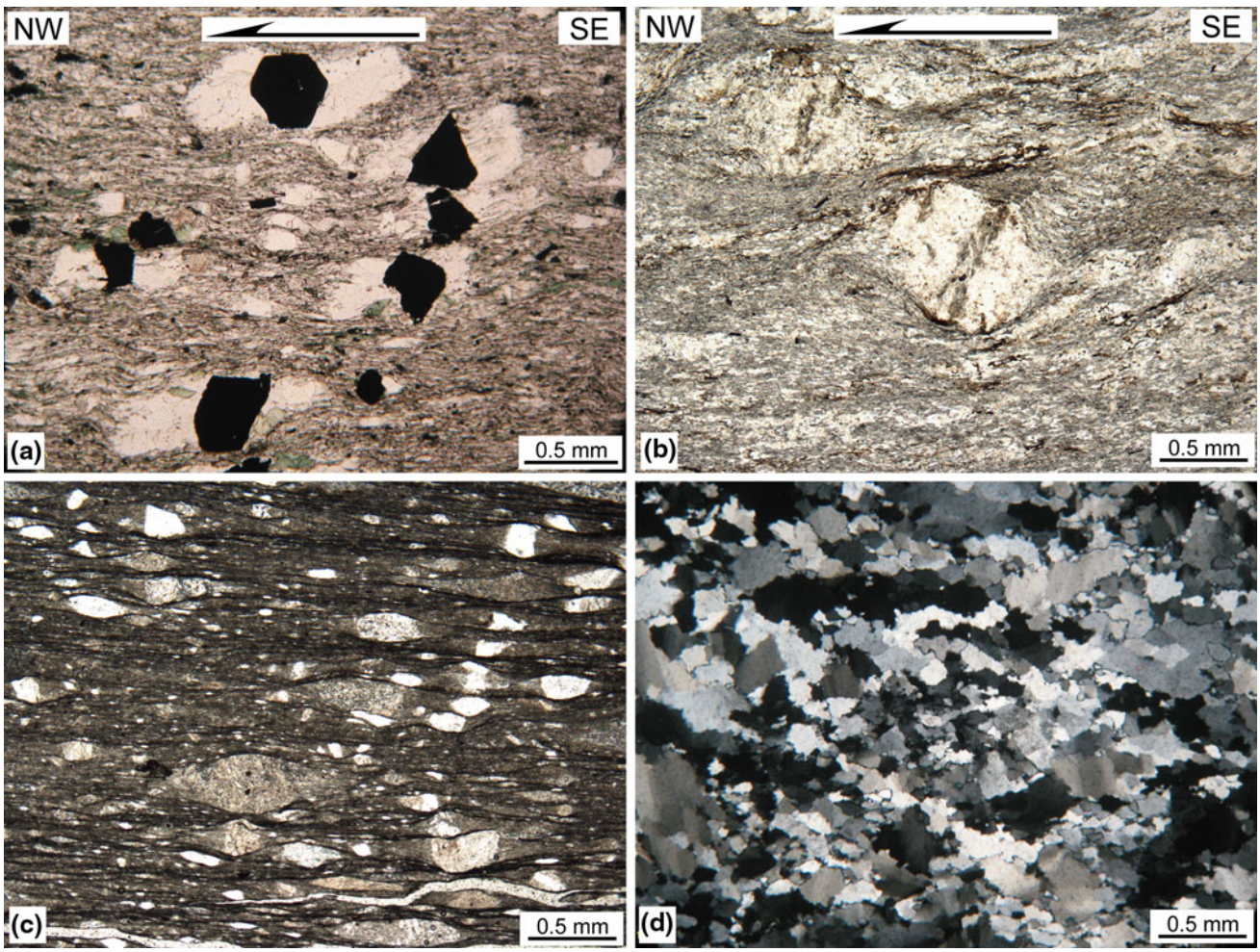

Fig. 9 Photographs showing the microscopic deformation of the Fengjia-Shuiche area. **a** Pressure shadows around pyrites in meta-sandstone showing the top-to-the-NW sense of shear, west of Simenqian. **b** Sigmoidal feldspar porphyroclasts in sandstone with a top-to-the-NW shear sense, east of Fengjia. **c** Strongly deformed meta-sandstone with oriented quartz grains showing dissolution along the grain long boundaries (perpendicular to the maximum shortening *Z* direction), and pressure shadows in the *X* direction, west of Fengjia. **d** Dynamically recrystallized quartz grains with serrated boundaries and oblique shape preferred orientation, east of Yanxi

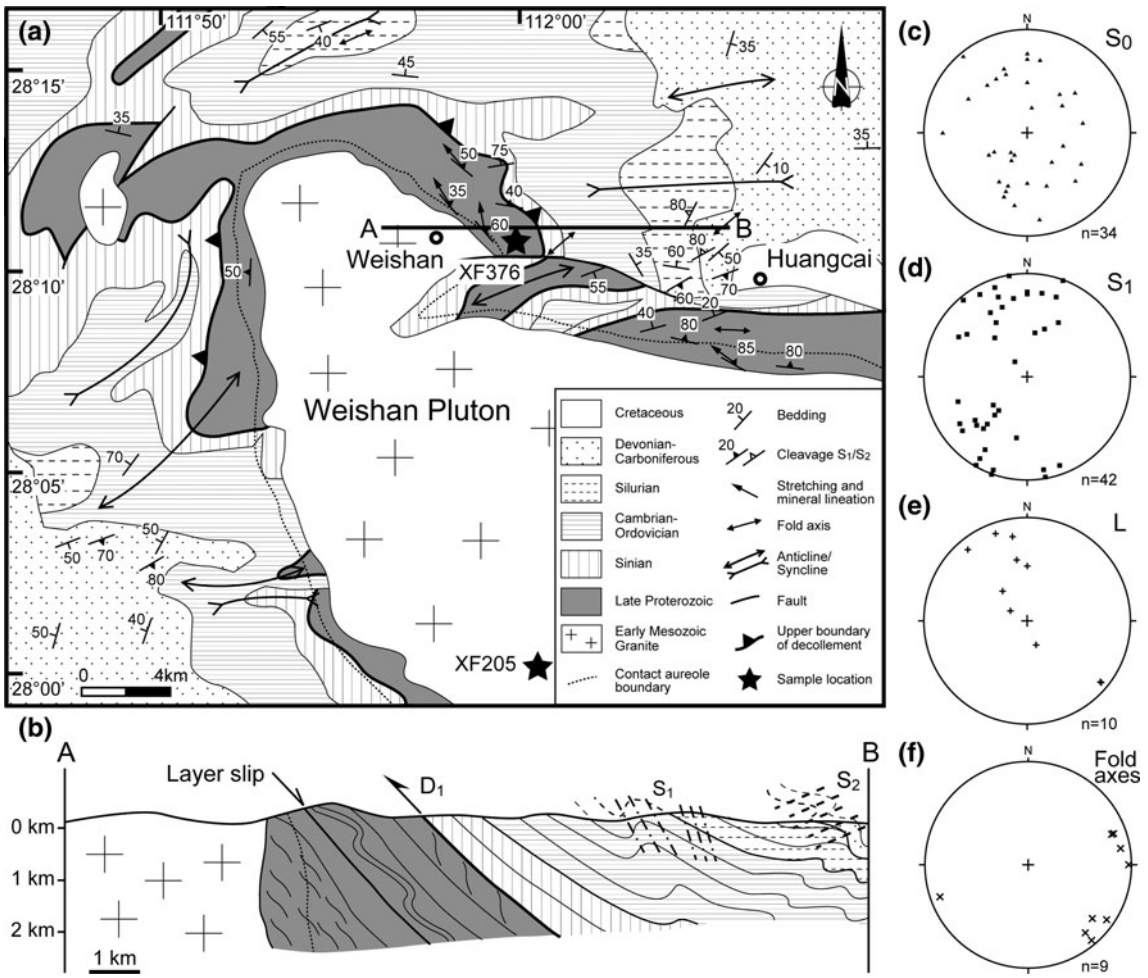

Fig. 10 **a** Detailed geologic map of the Weishan area (modified after 1:500,000 Geological map of Hunan, BGMRHN 1988). **b** Cross sections of the area. Stereographic plots (Schmidt lower hemisphere projection) of the structural elements, **c** bedding, **d** S_1 foliation, **e** stretching lineation, **f** fold axes

centimeter-scale gravels and fractured feldspathic pebbles (Fig. 8f). As described in the Chengbu area, in the vicinity of the Early Paleozoic pluton, andalusite formed by contact metamorphism during the granite intrusion is deformed along the direction of the regional lineation (Fig. 8g). The granitic pluton, especially south of Shuiche, is ductilely deformed and metamorphosed into orthogneiss. The mylonitic foliation is characterized by the alternation of light and dark layers corresponding to quartz–feldspar and biotite-rich parts, respectively (Fig. 8h). In some places, mafic enclaves are also elongated in the NW–SE direction. All the kinematic indicators are consistent with a top-to-the-NW ductile shearing.

Microfabrics

In thin sections cut in the *XZ* plane of the strain ellipsoid, deformation features are well developed. In the metapelite, quartz pressure shadows around pyrites, with fibers length ranging from ~0.1 mm to more than 0.5 mm long, develop with a consistent top-to-the-NW sense of shear (Fig. 9a). Top-to-the-NW kinematics is also evidenced by sigma-type feldspar porphyroclasts (Fig. 9b).

From outer to inner areas, the deformation mechanism changes from top to bottom of the décollement zone as mentioned above in the "Microfabrics" under the section "Chengbu area". In meta-sandstone and meta-conglomerate, quartz clasts are sheared and oriented parallel to the foliation. The participation of fluid, as shown by the development of foliation-parallel phyllosilicates, and pressure shadows along elongated clasts (Fig. 9b, c), indicates that the dominant deformation mechanism is pressure solution. This pattern agrees with low-temperature metamorphic conditions, and fluid circulation hampered intragranular deformation (Passchier and Trouw 2005). In the lower part of the décollement zone, polycrystalline aggregates, with grain size varying from ~50 to ~400 μm, exhibit a typical "core and mantle" texture

formed by dynamic recrystallization (Fig. 9d). Old, large clastic grains are replaced by elongate aggregates with numerous small neograins probably developed by subgrain rotation recrystallization. Locally, old grains are entirely replaced by a new grain network.

Thus, due to the increase in differential stress and temperature, intracrystalline slip turns to be the predominant deformation mechanism. In summary, similarly to the Chengbu area, the deepest observed part of the XFSB is exposed in the Fengjia-Shuiche area due to the uplifting of the Triassic pluton, and this litho-tectonic unit composed of lower greenschist facies metapelites and meta-sandstones is interpreted as the basal décollement zone that separates the ductilely deformed upper sedimentary cover series and the unexposed Proterozoic basement. Within this high-strain zone, the Neoproterozoic sedimentary rocks and the intruding early Paleozoic granites are changed into low-temperature mylonites and orthogneiss, respectively. Along the NW–SE trending lineation, various and abundant kinematic indicators argue for a top-to-the-NW shearing. At the grain-scale, diffusive mass transfer (i.e., pressure solution) appears as the main deformation mechanism, although in the deepest part of the décollement zone, dynamically recrystallized quartz aggregates suggest that intracrystalline plasticity becomes an important deformation mechanism.

Weishan area

The Weishan pluton is the largest Early Mesozoic granitic body cropping out in the XFSB. However, in this area, the well exposed, high-strain zone is restricted to the northeastern margin of the pluton (Figs. 1b, 10a). Above this zone, Sinian to Devonian sedimentary rocks are deformed both by the NW-verging D_1 and the D_2 SE-verging folds. To the west of the Weishan pluton, the regionally NE–SW striking D_1 fold axes turn to the NNE or N in the vicinity of the pluton. The Neoproterozoic meta-sandstone and micaschist are observed west and south of Huangcai (Fig. 10a). Due to the emplacement of the Weishan pluton, the original attitude of the foliation is modified to become parallel with the pluton boundaries, that is, the foliation dips to the NE and W in the northeastern and western borders, respectively (Fig. 10a). Moreover, a contact metamorphism aureole indicated by large, and randomly oriented biotite and muscovite grains develops around the entire granitic body. In order to avoid the influence of the contact metamorphism overprint, the macroscopic and microscopic observations have been done outside of the thermal aureole.

East of Weishan, in quartzite and micaschist, the foliation characterized by the preferred orientation of muscovite, biotite, and quartz grains dips to the N–NE (Fig. 10d). A NNW–SSE trending mineral and stretching lineation, expressed by oriented biotite and quartz aggregates, is consistent with the regional stretching lineation direction observed in the deformed sedimentary series of the XFSB (Fig. 10e). At the microscope scale, in meta-sandstone, clastic quartz grains with undulose extinction are elongated and, in some places, present a sigmoidal shape indicating a top-to-the-NW shearing. In quartzite, shear bands show a top-to-the-NW shear sense (Fig. 11a). Quartz aggregates consist of recrystallized grains with sutured or straight boundaries. An oblique shape fabric of the new grains, consistent with the top-to-the-NW sense of shear, can be observed (Fig. 11b). Locally, quartz grains exhibit a euhedral shape, planar grain boundaries, and triple junctions. These features suggest that the quartz aggregates experienced thermal annealing, likely during the development of the contact aureole coeval with the emplacement of the Weishan pluton. Nevertheless, our field and laboratory observations argue for the development of a syn-metamorphic, top-to-the NW, ductile shearing before the Weishan pluton intrusion. Moreover, in the metapelite, a fibrous sillimanite–muscovite assemblage argues for a high-temperature metamorphism predating the thermal aureole (Fig. 11c).

Shuangfeng area

Adjacent to the Ziyunshan pluton, ductilely deformed metamorphic rocks are well exposed in the pluton western margin, SE of Shuanfeng (Fig. 12a). In the study area, all the planar fabric elements, such as bedding, slaty cleavage, and metamorphic foliation, strike NE–SW (Fig. 12c, d). Away from the Ziyunshan pluton, SE-verging folds related to the D_2 event deform the Neoproterozoic to Devonian rocks. The sandstone and tillite formations are tilted, and become nearly vertical close to the pluton, and hereby post-intrusion collapse folds and layer slip normal brittle faults develop in limbs of anticlines, which are in agreement with a vertical shortening possibly related to granite emplacement (Fig. 11e, f). Micaschist and quartzite are less metamorphosed than in the previous three areas, but vertical planar cleavage (S_3) can be identified particularly along some folded quartz veins (Fig. 11d). Under the microscope, the bedding surface S_0 is superimposed by the S_1 cleavage (Fig. 11g). Although only weakly metamorphosed in this area, a contact metamorphic aureole marked by andalusite and biotite develops around the pluton. In contrast to the previous areas, the stretching lineation is weakly developed, and kinematic indicators are rare. This character can be understood by considering that the exposed metapelites correspond to the upper part of the décollement zone or alternatively that the linear structure and related kinematic indicators have

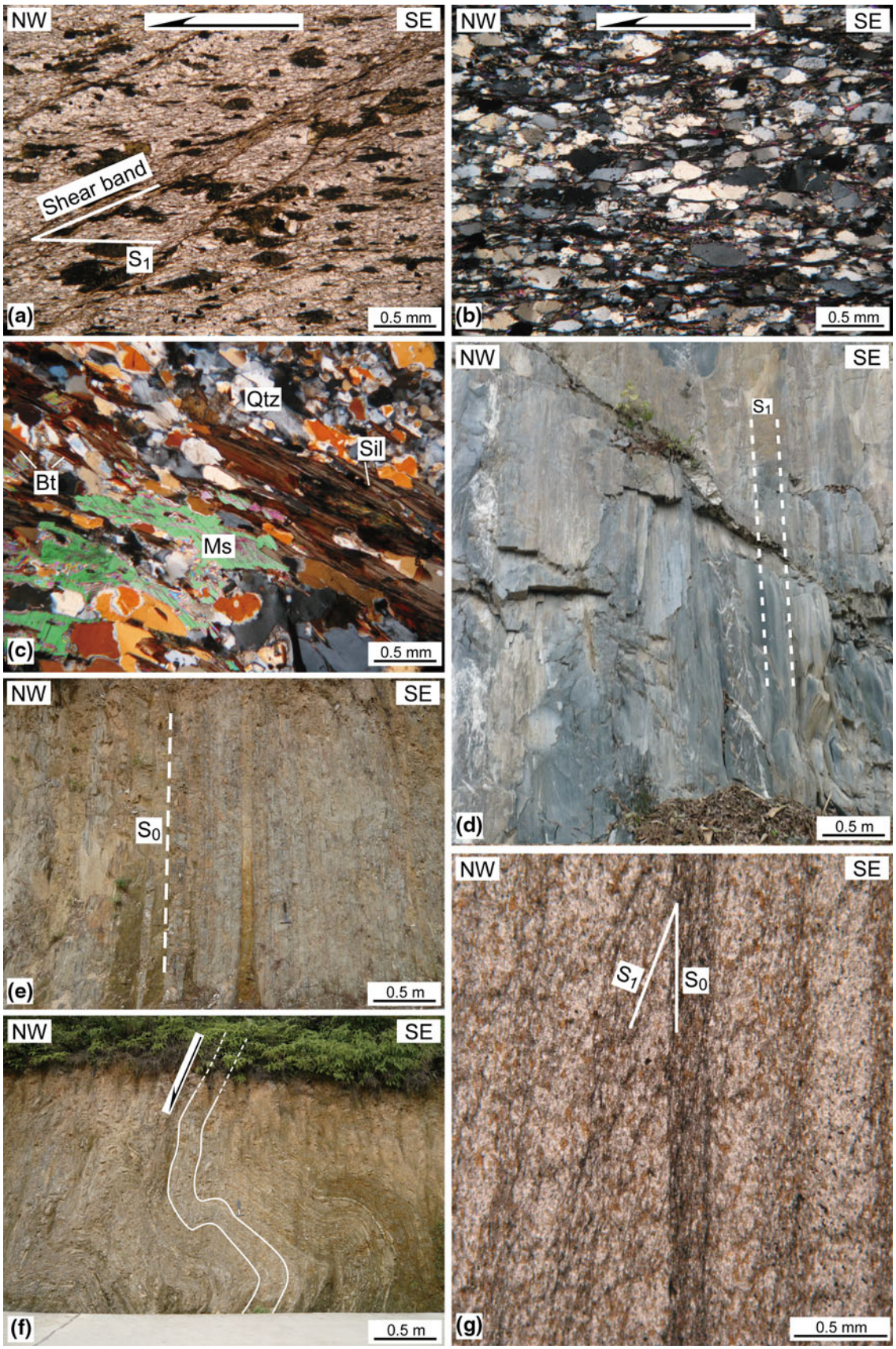
NW
SE
Shear band
S1
(a)
0.5 mm
NW
SE
(b)
0.5 mm
Qtz
Sil
Bt
Ms
(c)
0.5 mm
NW
SE
S1
(d)
0.5 m
NW
SE
S0
(e)
0.5 m
NW
SE
(f)
0.5 m
NW
SE
S1
S0
(g)
0.5 mm

◀ **Fig. 11** Photographs illustrating the deformation of Weishan and Shuangfeng areas. **a** Shear band structure with *horizontal* foliation and oblique shear plane, west of Huangcai. **b** Equigranular recrystallized quartz with several sigmoidal grains indicating a top-to-the-NW shearing, west of Huangcai. **c** Biotite (Bt)-sillimanite (Sil)-bearing micaschist with muscovite (Ms), and quartz (Qtz), west of Huangcai. **d** *Vertical* S_1 foliation in quartzite, east of Shuangfeng. **e** *Vertical* original bedding in pelite-sandstone alternation, southeast of Shuangfeng. **f** Gravitational collapse folds in Neoproterozoic sandstone, southeast of Shuangfeng. **g** Photo of original bedding (S_0) superimposed by cleavage (S_1), east of Shuangfeng

been erased by recrystallization, probably during the pluton emplacement.

In conclusion, the ductilely sheared metamorphic rocks exposed in the deepest part of the XFSB exhibit the same kinematic features as the D_1 structures developed in the Neoproterozoic to Early Triassic rocks. Thus, we interpret these sheared rocks as the basal ductile décollement zone that accommodated the NW-verging folds that result in shortening in the upper part of the orogen.

Geochronological constraints

In order to place time constraints on the ductile and syn-metamorphic deformation described above in the décollement zone, monazite U–Th–Pb dating of metamorphic rocks has been carried out. In addition, SIMS zircon U–Pb and monazite U–Th–Pb_{tot} dating have been performed on the granitoids that intrude into the basal décollement zone.

Sampling and analytical methods

During fieldwork, we collected samples for isotopic analyses, namely three granite samples for zircon SIMS U–Pb dating, and four granite samples and two micaschist samples for monazite Electron MicroProbe Analysis (EMPA) chemical dating. For SIMS dating, zircons were separated by conventional procedures using heavy liquids and a magnetic separator after concentration by hand panning. For EMPA chemical dating, monazites were analyzed

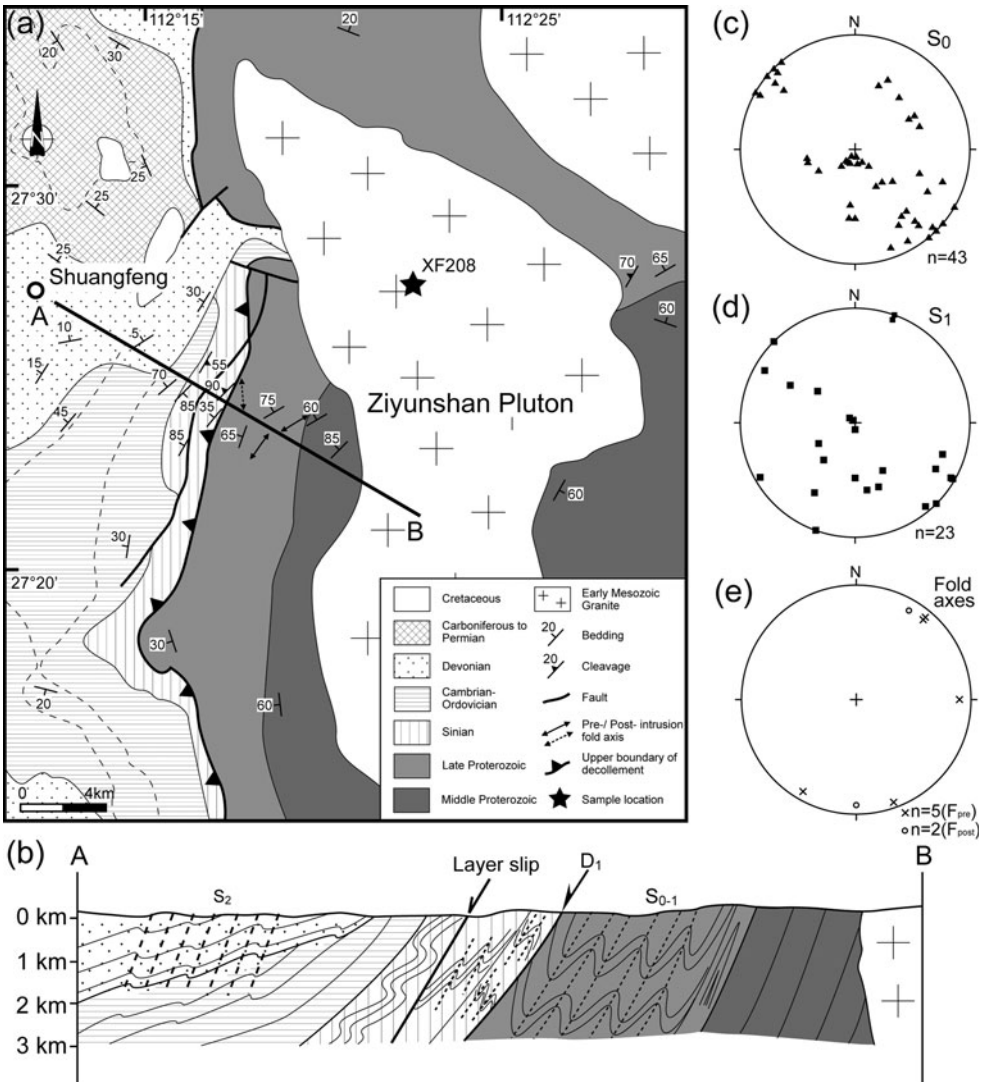

Fig. 12 **a** Detailed geologic map of Shuangfeng area (modified after 1:500,000 Geological map of Hunan, BGMRHN 1988). **b** Cross sections of the area. Orientation plots (Schmidt net, lower hemisphere) of the structural elements, **c** bedding, **d** S_1 foliation, **e** fold axes and crenulation lineation. F_{pre} and F_{post} fold axes before and after the intrusion of the pluton

directly on the polished thin section. A detailed description of both procedures is given in Appendix A.

Geochronological results of the metamorphic rocks in the basal décollement zone

Sample XF365

Sample XF 365 (N26°16.467′, E110°24.269′) is a garnet–muscovite–biotite–quartz–chlorite micaschist collected from the décollement zone in the Chengbu area. In thin section, the main fabric is the S_1 foliation with a top-to-the-NW shear sense shown by asymmetric pressure shadows around garnet porphyroblasts. Monazite grains are located in the matrix with chloritized biotite and range in size from 10 to 80 μm without zonation (Fig. 13a). The monazite grains are mostly prismatic with long axes parallel to the S_1 foliation; thus, we interpret these grains as synmetamorphic minerals crystallized during the D_1 ductile deformation. U–Th–Pb_{tot} electron probe analyses were performed in situ. This approach allowed us to select the largest and unzoned grains in contact with biotite that formed during the syn-D_1 metamorphic event. The Mean Square Weighted Deviation (MSWD) of 1.2 and the 74 data points are in agreement with a reliable single age. A weighted average age of 243 ± 9 is calculated and interpreted as the time of the ductile deformation (Fig. 14a).

Sample XF376

Sample XF376 (N28°11.317′, E111°58.108′) is a sillimanite–muscovite–quartz–biotite micaschist from the northeast of the Weishan pluton. Back-scattered electron images reveal that monazite grains are prismatic and range from 20 to 50 μm (Fig. 13b). Due to the low composition of radiogenic Pb, the calculated ages for single spot give a large error. Nevertheless, twenty-eight analyses in 13 grains yield a reliable weighted average age of 226 ± 18 Ma, with an acceptable MSWD of 0.95 (Fig. 14b). It is interpreted as the time of the amphibolite facies metamorphism coeval with the crystallization of sillimanite.

Geochronological results of granitic plutons

U–Th–Pb_{tot} monazite dating

Four granitic samples, XF205, XF208, XF326, and XF366, are selected for monazite dating. The monazite grains occur as inclusions in biotite and range in size from 50 to 500 μm (Fig. 13c–f). These monazite grains were analyzed directly from petrographic thin sections.

In sample XF205 (N28°00.255′, E112°00.455′), large ranges in Th/U indicate that the chemical composition is favorable for using the Th/Pb versus U/Pb diagram (Cocherie and Albarede 2001). Ninety-one analyses of seven grains yield well-defined intercept ages (U/Pb age: 222 + 24/−25 Ma and Th/Pb age: 239 ± 7 Ma). An isochron age of 236 ± 4 Ma is calculated at the centroid of the population (Fig. 14c).

Sample XF326 is a monzonitic granite collected from the Wawutang pluton (N26°46.013′, E110°20.266′). Sixty-eight spot analyses were performed on ten grains by using EPMA technique. Due to rather constant Th/U ratios, the spot analyses are clustered in the Th/Pb vs. U/Pb diagram (Fig. 14d), leading to large errors on the intercept ages (U/Pb age: 219 + 75/−87 Ma and Th/Pb age: 236 + 18/−16 Ma). Nevertheless, it is noteworthy that the slope of the regression line is very close to the theoretical isochron. A mean age of 233 ± 6 Ma was calculated at the centroid of the population.

Sample XF366 (N26°19.743′, E110°26.519′) is a gneissic granite collected from deformed Lanrong pluton. The constant Th/U ratio is not suitable for using the Th/Pb vs. U/Pb diagram to calculate a mean age. In such case, as the U + Th_{tot} concentration is very high and changes significantly, the most suitable diagram is that of Suzuki and Adachi (1991). All the analyses, with an intercept very close to the origin, yield a precise age at 414 ± 18 Ma (Fig. 14e), which is similar within errors to the result of zircon U–Pb dating method (XF314).

For sample XF208 (N27°27.802′, E112°22.327′), 82 analyses of six grains were performed. However, due to more concentrated Th/U ratios, neither the Th/Pb versus U/Pb diagram nor Pb–Th* diagram of Suzuki and Adachi is appropriate to calculate the mean age, a weighted average age of 230 ± 4 is preferred here to represent the timing of the emplacement (Fig. 14f).

U–Pb zircon dating

Sample XF205 is a biotite monzonitic granite collected from Weishan pluton. Concentric zoning is distinctly demonstrated in euhedral zircon, which is 100–250 μm in length with length–width ratios of 2:1–3:1 (Fig. 15a). Fourteen analyses on 14 zircons have 1,202–7,648 ppm of U, 192–2,176 ppm of Th, with 0.067–0.347 of Th/U ratios. Five spots with U contents over 4,000 ppm are discarded because of their abnormal old age related to high U. Similar phenomenon has also been reported during SIMS zircon U–Pb analyses (e.g., Li et al. 2010a). Hence,

Fig. 13 BSE (Back-scattered electron) images of the dated monazite grains without chemical zonation. **a** Garnet-bearing micaschist from the Chengbu area. **b** Biotite-sillimanite-bearing micaschist from the Weishan area. **c** Weishan granite. **d** Ziyunshan granite. **e** Wawutang granite. **f** Lanrong deformed granite ▶

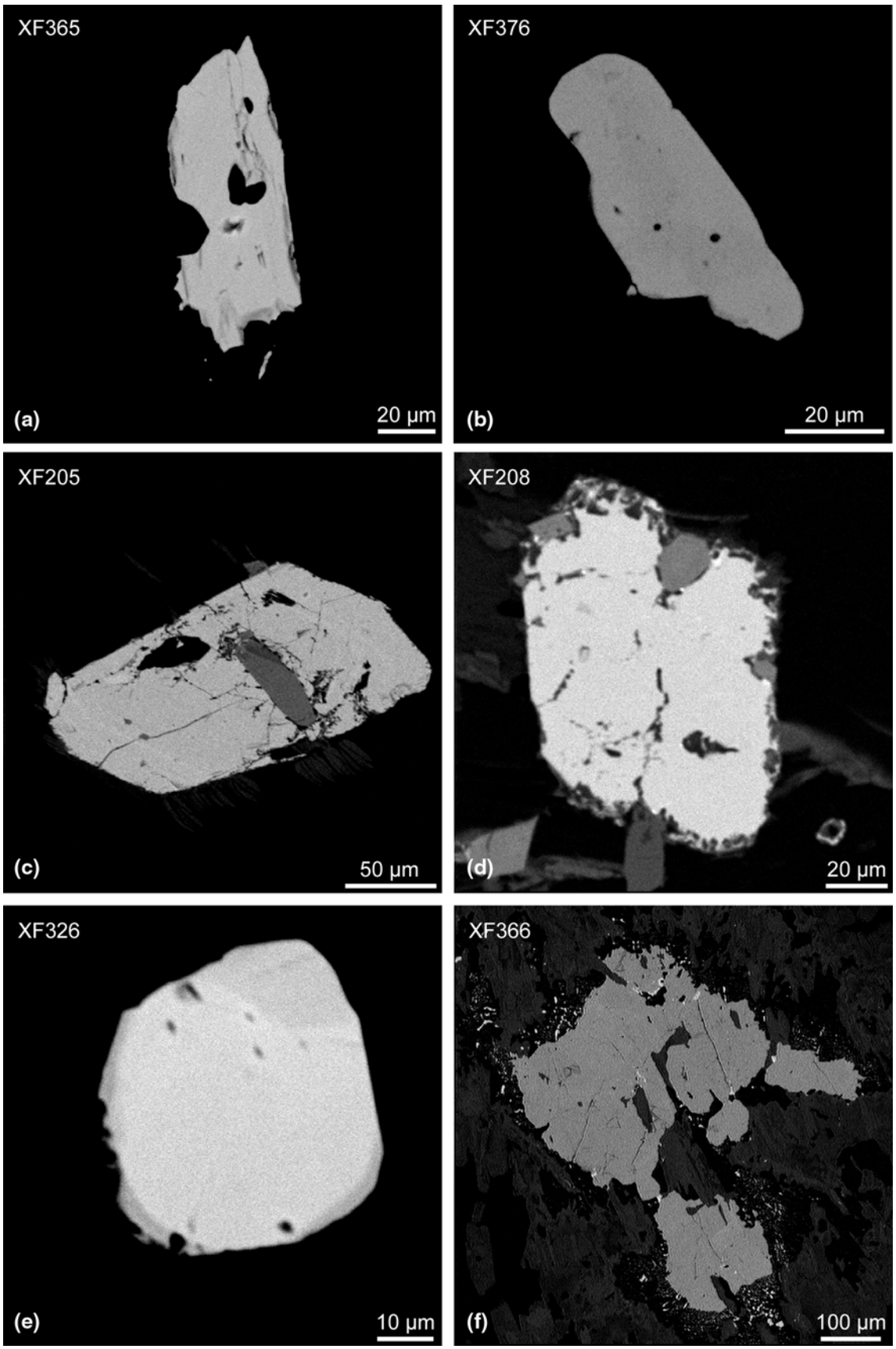
XF365
(a)
20 μm
XF376
(b)
20 μm
XF205
(c)
50 μm
XF208
(d)
20 μm
XF326
(e)
10 μm
XF366
(f)
100 μm

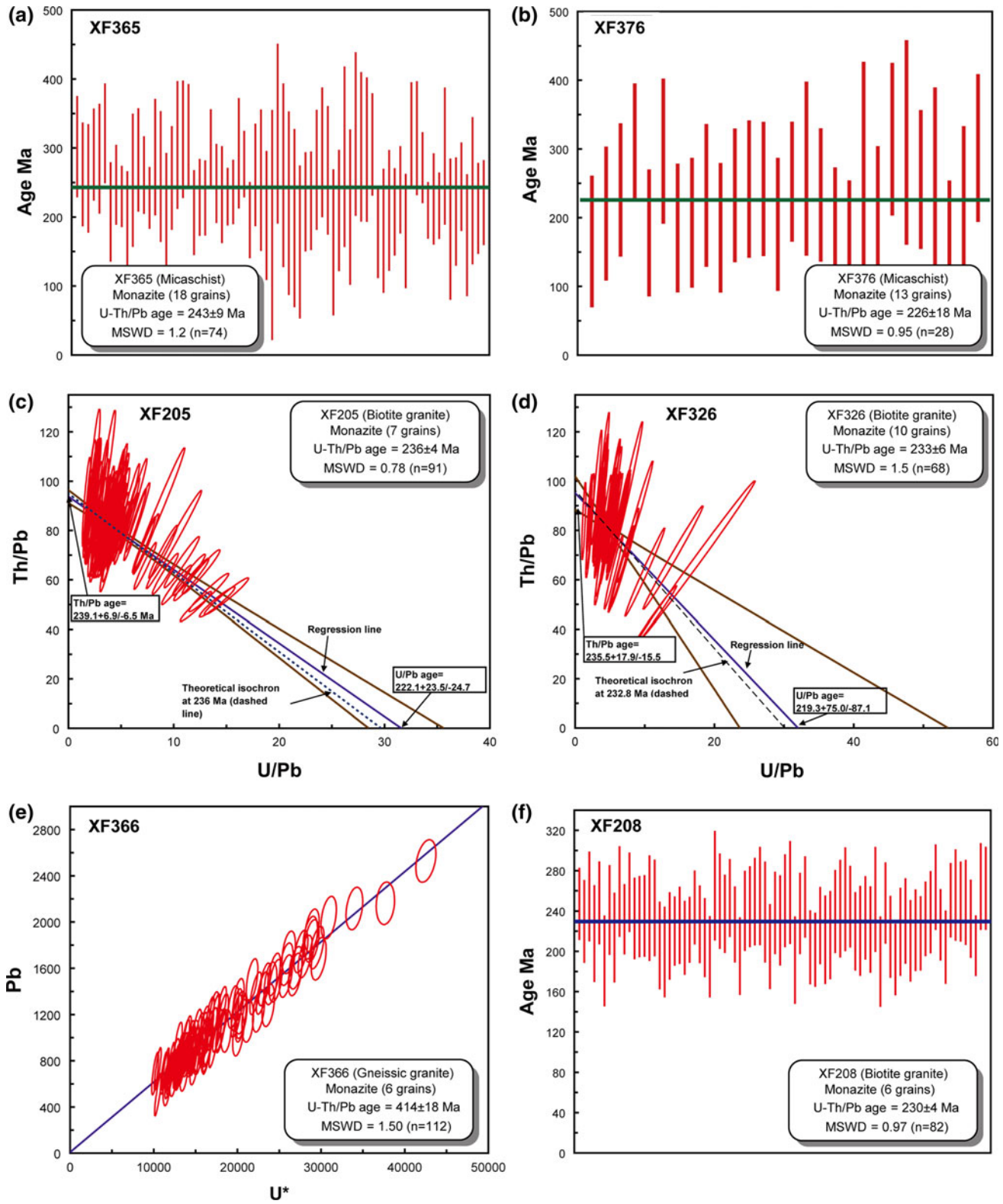

Fig. 14 Diagrams of monazite U–Th–Pb dating results. **a** Garnet-bearing micaschist from the Chengbu area. **b** Biotite-sillimanite-bearing micaschist from the Weishan area. **c** Weishan granite. **d** Ziyunshan granite. **e** Wawutang granite. **f** Lanrong granite

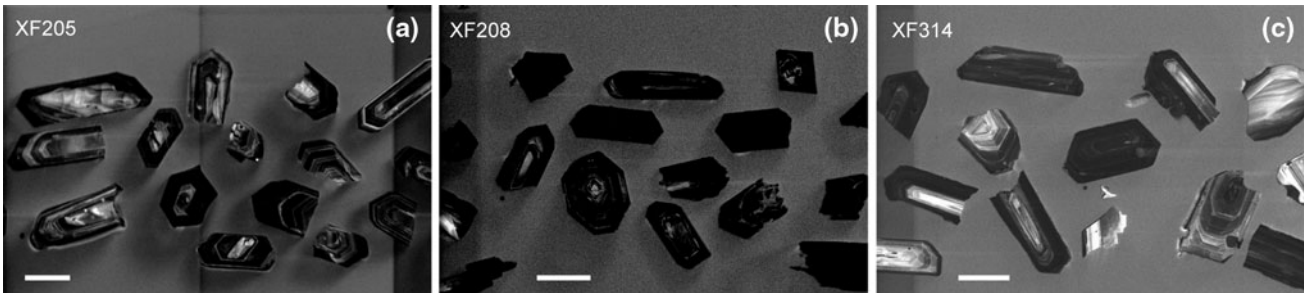

Fig. 15 Examples of cathodoluminescence images of the dated zircons from samples XF205, XF208 and XF314

excluding these five spots, the other nine analyses yield a Concordia $^{206}Pb/^{238}U$ age of 222 ± 3 Ma (Fig. 16a), which likely represents the pluton emplacement age.

Sample XF208 is a two-mica granite collected from Ziyunshan pluton. Relatively transparent and colorless, euhedral or subhedral zircons with concentric zoning are commonly observed in this sample (Fig. 15b). Zircons are 50–150 μm long with length–width ratios of 1:1–2:1. Fourteen analyses on 14 fourteen zircons, with 851–1,603 ppm of U, 172–817 ppm of Th, and 0.203–0.538 of Th/U ratios, give indistinguishable U–Pb isotopic compositions within errors, which correspond to a single-age population with a Concordia $^{206}Pb/^{238}U$ of 226 ± 2 Ma (Fig. 16b), corresponding to the intrusion of Ziyunshan pluton.

Sample XF314 is a gneissic granite collected from Lanrong pluton beside the location of sample XF366. Zircons from this sample are mostly subhedral to anhedral and 50–200 μm long with mostly 2:1–3:1 of length–width ratios (Fig. 15c). Fifteen analyses of fifteen zircons were performed, with 163–1,581 ppm of U, 195–500 ppm of Th, 0.280–1.322 of Th/U ratios, and a Concordia age of 418 ± 3 Ma (Fig. 16c). This Paleozoic age represents the crystallization age of this pluton.

All the U–Pb age results are presented in Appendix B.

Discussion

Summary of the deformational characteristics in the basal décollement zone

The Xuefengshan intracontinental belt experienced a polyphase deformation with a dominant D_1 phase of top-to-the-NW compression and shearing, followed by a subsequent SE-verging back-folding and back thrusting D_2 phase, and lastly a D_3 phase of upright folding (Wang et al. 2005; Chu 2012). As three events form a continuum of deformation, D_1, D_2, and D_3 phases developed under the Early Mesozoic compression that led to the formation of the XFSB. Among these three events, D_1 is the main one that controls the architecture of the belt. Although less penetrative, the D_2 and D_3 structures play an important role in modifying the D1 structures and shaping the final structural pattern of the XFSB (Chu 2012). Neoproterozoic to Early Triassic sedimentary rocks, with rarely developed lower greenschist facies metamorphism, were intensely deformed. In addition, the possibility of intrusion-related deformation can be excluded as similar shear sense occurs in the high-strain zone and sedimentary cover on the both limbs of anticlines with granitoid cores. However, unlike many orogenic belts, high-grade metamorphic rocks, like amphibolite or migmatite, are absent in this belt (BGMRHN 1988). In order to accommodate the shortening observed in shallow crustal rocks, a basal décollement zone must have developed at depth within ductilely deformed metamorphic rocks. Such a décollement zone crops out in the core of anticlines formed during the emplacement of post-tectonic Late Triassic plutons. As shown above, a flat-lying foliation, a NW–SE stretching lineation, and a top-to-the-NW shearing characterize the ductile deformation. Thus, this ductile deformation recorded in the basal décollement zone can be correlated to the D_1 event recognized in the sedimentary cover.

As exemplified by the Alpine Jura or Zagros Fold-and-Thrust Belt, high-strain décollement zones are well developed in the outer zone of collisional belts. They are commonly represented by low strength rocks, such as evaporites or black shales (Escher and Beaumont 1997; McQuarrie 2004). Below the basal décollement zone, basement rocks lack strong and pervasive deformation. In the XFSB, the main crustal décollement located at the base of the Proterozoic to Early Triassic sedimentary series allows the NW–SE shortening recorded by the D_1 event to be accommodated at depth. Furthermore, a basal thrust or detachment has been assumed in the previous studies (Qiu et al. 1999; Wang et al. 2005), and thus, the existence of a ductile décollement zone, indicating decoupling within the crust, is consistent with the bulk architecture of the XFSB.

In the décollement zone, the flat-lying foliation, NW–SE striking stretching lineation, and intrafolial folds developed during a top-to-the-NW shearing, as documented by numerous kinematic indicators. Paleozoic granites were

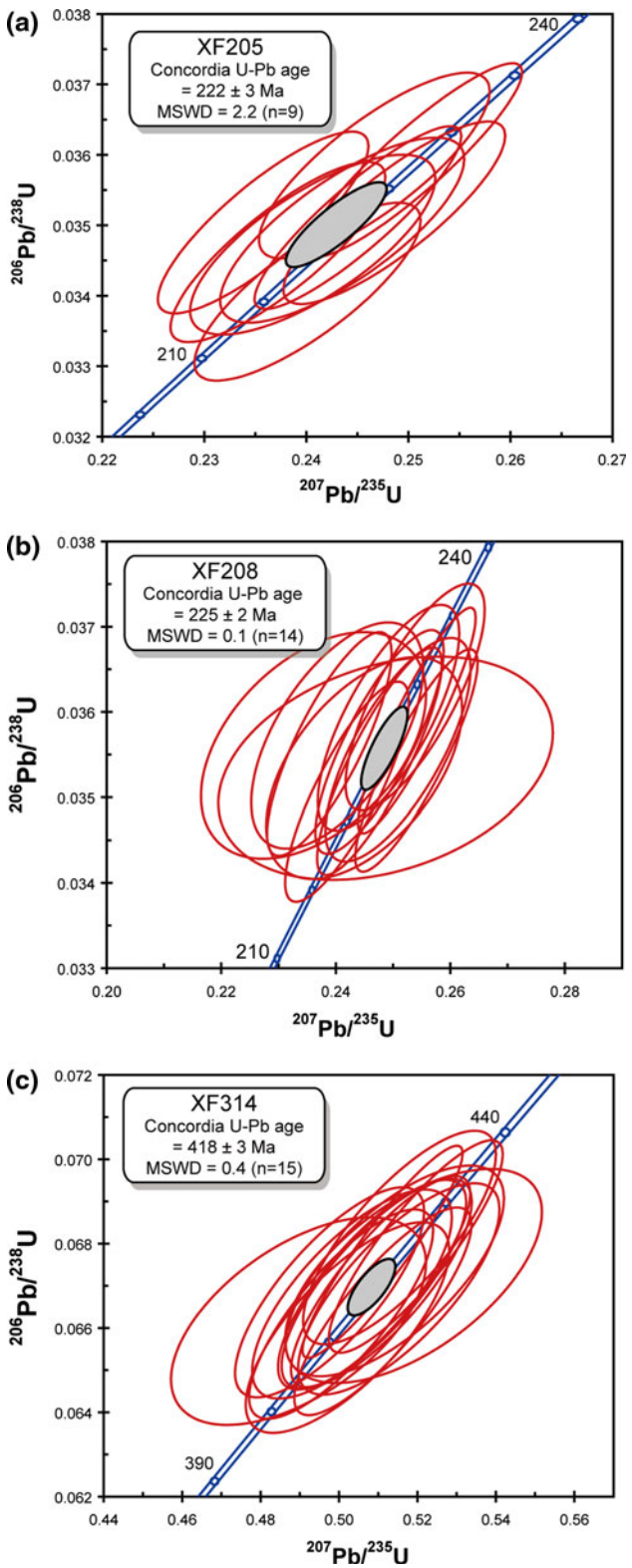

Fig. 16 Concordia diagrams of SIMS zircon U–Pb data. **a** Weishan granite. **b** Ziyunshan granite. **c** Lanrong granite

also involved in this shearing, producing orthogneiss and mylonites in the pluton margins. Although observed around the Late Triassic post-orogenic plutons, the ductile deformation of the metamorphic rocks appears to predate the pluton emplacement. The flat-lying foliation that extends several kilometers away from the pluton is not in agreement with a deformation that would be uniquely related to a forceful emplacement. Obviously, the rocks involved in the décollement zone were deformed by D_3 event like other series located above the décollement zone. At the microscope scale, pressure solution appears as the main deformation mechanism responsible for the development of the ductile fabrics under low-grade metamorphic conditions. However, in the deepest parts of the décollement, the ductile deformation increases as indicated by quartz microstructures and quartz *c*-axis fabrics. All the diagrams indicate that quartzite and micaschist mylonites developed at low temperature (ca. 300–400 °C) where pressure solution is the dominant mechanism, and dislocation glide and dynamic recrystallization become effective when temperature increases (Tullis et al. 1973; Stipp et al. 2002; Passchier and Trouw 2005).

Ductile deformation and crustal melting in the Xuefengshan Belt

The monazite U–Th–Pb_{tot} and the zircon U/Pb ages presented above provide new time constraints on the evolution of the XFSB. In spite of large uncertainty, monazites from micaschist of the basal décollement zone yield a chemical age range of 243–226 Ma, indicating that the top-to-the-NW shearing occurred during the Middle Triassic.

The Triassic aluminous to peraluminous plutons, which intrude already deformed rocks, are widely distributed across the XFSB (Fig. 1b). Although these granites are dated with different isotopic methods, the age of magmatism is still controversial (Ding et al. 2005; Chen et al. 2006, 2007a, b; Wang et al. 2007a; Li and Li 2007; Li et al. 2008). The synthesis of the available age data is shown in Fig. 17. Our zircon U–Pb and monazite U–Th–Pb_{tot} geochronological data allow us to narrow the time interval of the magmatic activity in the XFSB. These new time constraints show that pluton emplacement occurred in the Late Triassic, at the end of the orogeny.

It is worth noting that the monazite U–Th–Pb age, at ca. 226 Ma, of the biotite–sillimanite micaschist (sample XF 376) picked around the Weishan pluton is close to the monazite and zircon ages of the undeformed granites that postdate the activity of the basal décollement zone. Nevertheless, the closure temperature of the monazite U–Pb system (725 ± 25 °C) is higher than that of the thermal contact metamorphism. From the structural point of view, these monazites grains have a shape preferred orientation parallel to the S1 foliation, and monazite long axes are parallel to the lineation. This fabric features

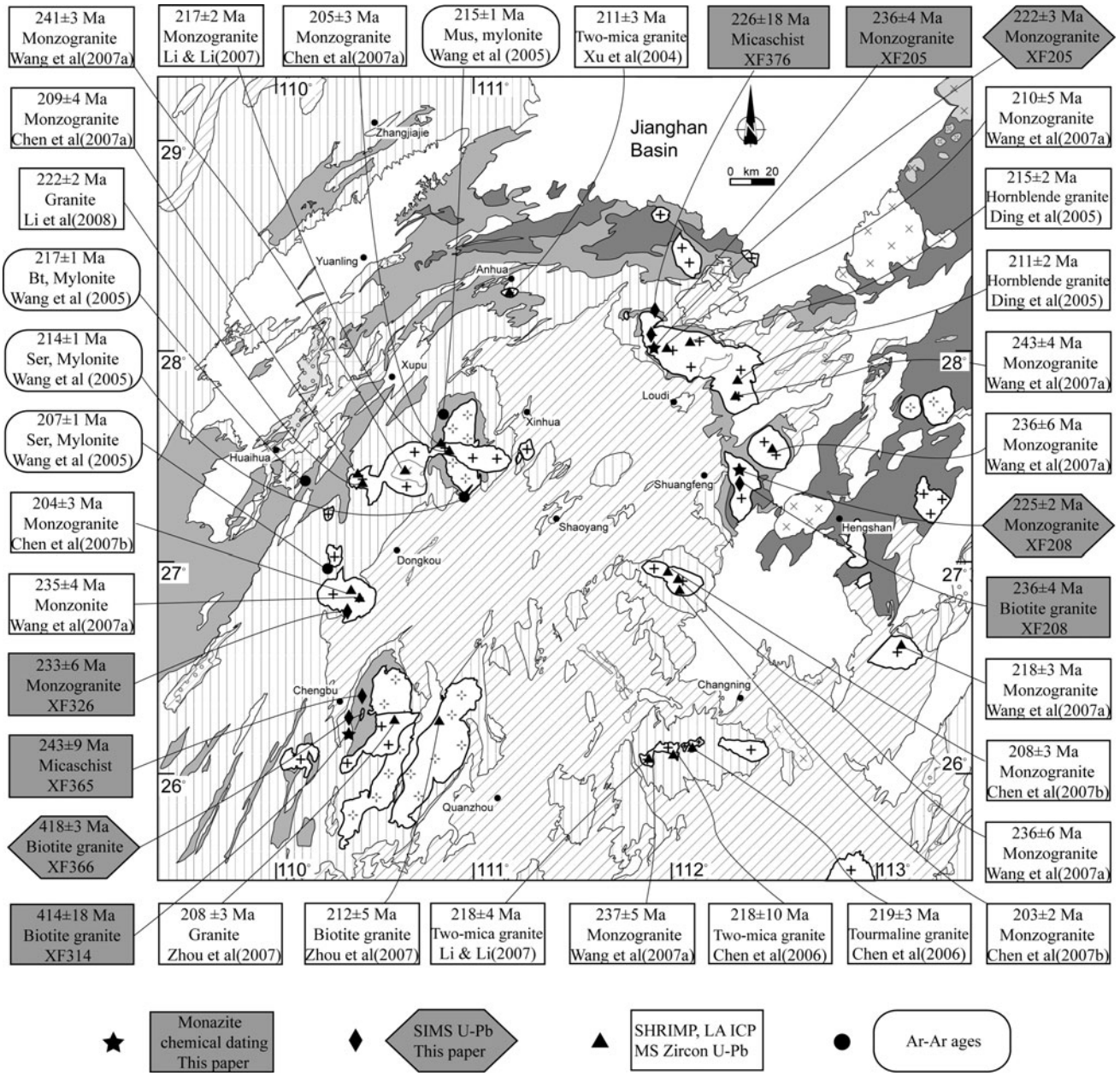

Fig. 17 Synthetic map of the Xuefengshan Belt showing the available radiometric data

indicate that monazite crystallization is coeval with deformation. In addition, these monazite grains lack any optical or chemical zonation that would support a two-stage evolution interpretation, with an initial crystallization followed by a recrystallization responsible for age resetting. Therefore, we interpret the U–Th–Pb_{tot} age as that of a deformation event. This biotite–sillimanite rock argues for a high temperature syn-tectonic metamorphism that might be developed as a consequence of the thermal event responsible for crustal melting and the emplacement of the Triassic granites at the end of the Xuefengshan orogeny.

Tectonic evolution of the XFSB

As already described, the SCB experienced a ductile deformation, middle-high-grade metamorphism, and widespread crustal partial melting during the Early Paleozoic orogeny in Late Ordovician to early Silurian (Faure et al. 2009; Li et al. 2010b; Charvet et al. 2010). However, the XFSB was almost not influenced by this event, except in the southeastern part of the region (Fig. 1). Most of the regional faults, cleavage or foliation directions, fold axial planes are trending NE–SW, and the deformation pattern of the XFSB are consistent in both pre- and post-Devonian

rocks, including the entire Paleozoic series, and the Early and Middle Triassic one. The Late Triassic, Jurassic, and Cretaceous rocks that unconformably overly the deformed series place a time constraint on the deformation. The geometric and kinematic consistency between the Paleozoic and Early Triassic rocks shows that the structure of the XFSB is the product of the same deformation event, i.e., the Early Mesozoic Orogeny. Furthermore, a very significant criterion to distinguish the Early Mesozoic structures from the Early Paleozoic ones is that the Early Paleozoic granites that represent the post-orogenic plutons of the Early Paleozoic orogen are ductilely deformed into orthogneiss when involved into the Early Mesozoic Orogeny (Wang et al. 2005, 2007b; Xu et al. 2011). Moreover, the Early Mesozoic granites are not deformed. In the country rocks around the Paleozoic plutons, contact metamorphism andalusite was reoriented during the Early Mesozoic D_1 event. Wang et al. (2005) have obtained five sericite and biotite ^{40}Ar–^{39}Ar data between 217 and 195 Ma and explained them as ductile shearing age. However, combined with the above-mentioned lines of evidence, these ages can represent a cooling stage of the orogens, as the ^{40}Ar–^{39}Ar ages are younger than that obtained for the emplacement of the non-deformed, post-orogenic granites.

Geodynamic significance of the XFSB in the SCB tectonic framework

Our detailed, multi-scale structural analysis and geochronological study on monazite and zircon allow us to clarify the deformation pattern in the décollement zone and the timing of the orogen. The regional top-to-the-NW ductile shearing coeval with folding and thrusting dominated the architecture of the XFSB.

An Early Paleozoic orogeny has been proposed (Qiu et al. 1998, 1999), but the available stratigraphic and radiometric constraints do not support this view, since the Devonian to Early Triassic rocks are deformed with the same structural features. Wang et al. (2005) proposed an asymmetric, positive flower-shaped, transpressional model to explain the ductile shearing with a sinistral strike-slip component. Based on stratigraphic and geochronological data, the main deformation occurred between the Late Triassic and early Jurassic, but our structural studies do not support the sinistral flower-shaped transpressional model. Indeed, in the XFSB, strike-slip faults are brittle structures, cutting through the undeformed granitic plutons, indicating a pre-Late Triassic event. Yan et al. (2003) interpreted the XFSB as the result of the westward progressive collision of the Yangtze Block with the North China Block during the Late Jurassic to Cretaceous, but in this model, the Triassic event, which is clearly postdated by the Late Triassic plutons and the regional Late Triassic unconformity, is taken into account. Additionally, evidence for a Late Triassic–Early Jurassic deformation in the XFSB is lacking.

Although the general tectonic interpretation of the belt is still controversial (Qiu et al. 1998, 1999; Yan et al. 2003; Wang et al. 2005), the structural analysis of the décollement presented above argue for a large-scale thin-skinned tectonic model with a high-strain basal décollement zone, rooted in the Chenzhou-Linwu Fault, between the sedimentary cover and basement rocks (Fig. 18a, b). West of the Chenzhou-Linwu Fault, the XFSB is characterized by NE–SW trending structures. In order to accommodate the shortening experienced by the Late Neoproterozoic (Sinian) to Early Triassic sedimentary series, the underlying basement must have experienced an intracontinental underthrusting to the SE during the Triassic (Fig. 18a).

To the east, in Jiangxi province, well-preserved Early Paleozoic structures, interpreted as an intracontinental orogen (Faure et al. 2009), are weakly reworked by the Triassic deformation. Furthermore, Early Paleozoic deformations in the XFSB are poorly constrained. Based on our observation, these structures are only locally developed in the southern part of the belt. We thus propose that the Chenzhou-Linwu Fault acted as a buttress or back-stop during the formation of the west-directed fold-and-thrust belt, which separates the Early Mesozoic and Early Paleozoic tectonic domains. As a significant boundary at the scale of the entire SCB, the Chenzhou-Linwu fault is regarded as the Neoproterozoic suture zone between the Yangtze block and the Cathaysia block. This fault is thus an inherited weak crustal zone, reactivated during the Triassic Xuefengshan orogeny. This distinct discontinuity represented by the fault is also documented by seismic data (Wang et al. 2003; Zhang and Wang 2007).

During the Early Triassic, the SCB underwent several orogenic events along its boundaries. To the north, the SCB subducted beneath the North China Craton (Hacker and Wang 1995; Faure et al. 1999, 2008); to the northwest, the Songpan-Ganzi and Longmenshan Belts record evidence for a Triassic deformation (Wallis et al. 2003; Harrowfield and Wilson 2005; Roger et al. 2008, 2010); to the west, the Jinshajiang suture zone is characterized by east-directed deformation (Wang et al. 2000); and to the southwest, the Yunnan-Guangxi-NE Vietnam Belt separates the SCB from Indochina (Carter et al. 2001; Carter and Clift 2008; Lepvrier et al. 2011). Nevertheless, none of these orogens is directly related to the intracontinental XFSB. The fact that the NE–SW trending XFSB is almost perpendicular to the Dabie orogen to the north and the Indosinian orogen to the south shows little geodynamic interaction between these belts. Moreover, because the displacement direction of deformation of the XFSB is opposite to that of the Songpan-Ganzi Belt, it is thus difficult to attribute the formation of the XFSB to the Dabie orogen and the Songpan-Ganzi Belt.

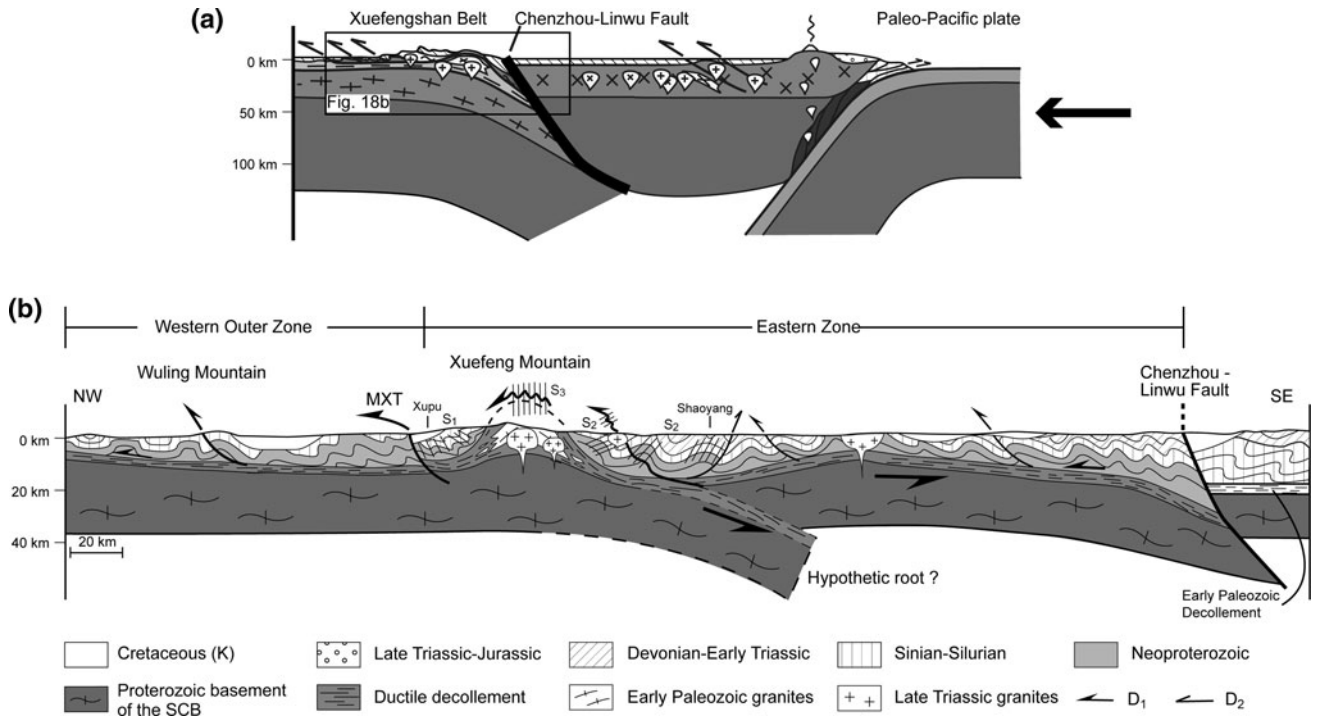

Fig. 18 **a** General tectonic model of the South China block in the Early Mesozoic. The hypothetic second subduction is not presented here. **b** Schematic bulk cross section of the Xuefengshan Belt: the Triassic basal décollement, observed in the core of the D_3 anticlines, separates the upper crust deformed by NW-directed folding and thrusting, and the middle-lower crust deepening to the SE. The Xuefengshan Belt is intruded by late Triassic peraluminous granitic plutons. East of the Chenzhou-Linwu fault, the Triassic deformation is weak. The main structure developed during the Early Paleozoic orogeny corresponds to South or SE-verging folds underlain by a décollement (e.g. Faure et al. 2009). One décollement is depicted rooted in the Chenzhou-Linwu fault. SE of Shaoyang, due to the second phase of top-to-the-SE shearing, the décollement is cut by a D_2 SE-directed thrust coeval with S_2 cleavage

During the Mesozoic, Triassic granitic rocks are widespread not only in the XFSB, but also throughout the entire SCB (Faure et al. 1996; Xu et al. 2004; Deng et al. 2004; Li and Li 2007; Wang et al. 2007b; Zhou 2007; Lin et al. 2008). A flat slab subduction model has been brought forward to account for the inland-directed propagation of Triassic plutonism (Li and Li 2007; Kusky et al. 2010). This model may generate a volume of magma scattered in a wide area in the upper plate of the subduction system. Such a mechanism is often invoked to account for the Laramide orogen in the Western North American Cordillera, and the Andes in South America (Haschke et al. 2002; English and Johnston 2004). However, this model is still in testing for the SCB, as the onset of the Pacific plate subduction remains in debate, and the spatial and temporal distribution of the Triassic magmatism does not show a clear regional trend (Engebretson et al. 1985; Ding et al. 2005; Chen et al. 2006, 2007a, b; Li et al. 2006, 2008; Wang et al. 2007a; Li and Li 2007). Additionally, taking into account that the deformation in southeastern South China is coeval with or even younger than the tectonics in the XFSB (Chen 1999), a progressive deformation is questionable.

As well exemplified by the Petermann and Alice Springs orogens of Australia, a weak crustal zone, such as a fault, an old suture, or a rift, might be easily reactivated during a subsequent intracontinental orogeny (Hand and Sandiford 1999; Holdsworth et al. 2001; Sandiford et al. 2001). The reactivation of the Chenzhou-Linwu fault zone in the SCB is a possible interpretation for the localization of the XFSB. After the completion of the Early Neoproterozoic Jiangnan orogeny that produced the welding of the Yangtze and Cathaysia blocks, the development of rifts within the newly formed South China Block was a suitable setting to accumulate more than 10-km-thick Neoproterozoic terrigeneous sediments followed by black shales and limestones, and finally covered by Silurian turbidite series that corresponds to the erosion of the early Paleozoic orogen (BGMRJX 1984; BGMRGX 1985; BGMRHN 1988; Faure et al. 2009; Charvet et al. 2010).

During the Early Mesozoic, the deformation experienced by SCB might likely be related to the Paleo-Pacific subduction, although precise constraints are not available. At that time, the Chenzhou-Linwu Fault, which represents an old inherited structure, was easily reactivated. As a consequence, the intracontinental contraction generated

the top-to-the-NW thrusting and folding of the sedimentary cover in the XFSB, and the basal ductile décollement zone accommodated at depth the crustal shortening (Fig. 18a).

Conclusion

The XFSB represents an example of an intracontinental orogen in which the shortening represented by NW-verging folding and thrusting is well developed in the Neoproterozoic to Early Triassic sedimentary series. At depth, this deformation is accommodated by a basal ductile décollement with a pervasively developed, synmetamorphic top-to-the-NW shearing. The monazite U–Th–Pb_{tot} chemical dating is in agreement with a Triassic age for the synmetamorphic ductile deformation. Widespread plutons, which cut the Early Mesozoic structures, are dated by zircon U–Pb method. Based on these results, the formation of the XFSB occurred between 245 and 215 Ma, with NW-directed folding, thrusting and shearing around 245–226 Ma, and emplacement of late-orogenic granites at 235–215 Ma.

Acknowledgments Field works have been funded by the Innovative Project of the Chinese Academy of Sciences (Grant No. KZCX1-YW-15-1) and Major State Basic Research Development Program of China (2009CB825008). National Natural Science Foundation of China grants no 90714007 and 40730315 are also acknowledged. A. Cocherie is thanked for his advices in processing the U–Th–Pb monazite data. Editor-in-Chief Wolf-Christian Dullo, Associate-Editor Wenjiao Xiao, Bei Xu and Claude Lepvrier are thanked for constructive comments. T. Kusky is also acknowledged for his help to improve an early draft of this manuscript.

References

Avouac JP, Tapponnier P, Bai M, You H, Wang G (1993) Active thrusting and folding along the northern Tien Shan and late Cenozoic rotation of the Tarim relative to Dzungaria and Kazakhstan. J Geophys Res 98:6755–6804

Bureau of Geology and Mineral Resources of Fujian Province (BGMRFJ) (1985) Regional geology of the Jiangxi Province. Geological Publishing House, Beijing, pp 1–671

Bureau of Geology and Mineral Resources of Guangxi province (BGMRGX) (1985) Regional geology of the Guangxi Zhuang autonomous region. Geological Publishing House, Beijing, pp 1–853

Bureau of Geology and Mineral Resources of Hunan province (BGMRHN) (1988) Regional geology of the Hunan Province. Geological Publishing House, Beijing, pp 1–719

Bureau of Geology and Mineral Resources of Jiangxi Province (BGMRJX) (1984) Regional geology of the Jiangxi Province. Geological Publishing House, Beijing, pp 1–921

Bureau of Geology and Mineral Resources of Zhejiang Province (BGMRZJ) (1989) Regional geology of the Jiangxi Province. Geological Publishing House, Beijing, pp 1–688

Carter A, Clift PD (2008) Was the Indosinian orogeny a Triassic mountain building or a thermotectonic reactivation event? Comptes Rendus Geosci 340:83–93

Carter A, Roques D, Bristow C, Kinny P (2001) Understanding Mesozoic accretion in Southeast Asia: significance of Triassic thermotectonism (Indosinian orogeny) in Vietnam. Geology 29: 211–214

Charvet J, Shu LS, Shi YS, Guo LZ, Faure M (1996) The building of south China: Collision of Yangzi and Cathaysia blocks, problems and tentative answers. J Southeast Asian Earth Sci 13: 223–235

Charvet J, Shu LS, Faure M, Choulet F, Wang B, Lu HF, Le Breton N (2010) Structural development of the Lower Paleozoic belt of South China: genesis of an intracontinental orogen. J Asian Earth Sci 39:309–330

Chen A (1999) Mirror-image thrusting in the South China Orogenic Belt: tectonic evidence from western Fujian, southeastern China. Tectonophysics 305:497–519

Chen WF, Chen PR, Zhou XM, Huang HY, Ding X, Sun T (2006) Single-zircon La-ICP-MS U-Pb dating of the Yangmingshan granitic pluton in Hunan, South China and its petrogenetic study (in Chinese with English abstract). Acta Geol Sinica 80:1065–1077

Chen WF, Chen PR, Huang HY, Ding X, Sun T (2007a) Chronological and geochemical studies of granite and enclave in Baimashan pluton, Hunan, South China. Sci China (D) 50: 1606–1627

Chen WF, Chen PR, Zhou XM, Huang HY, Ding X, Sun T (2007b) Single zircon LA-ICP-MS U-Pb dating of the guandimiao and wawutang granitic plutons in Hunan, South China and its Petrogenetic significance. Acta Geol Sinica 81:81–89

Chen CH, Hsieh PS, Lee CY, Zhou HW (2011) Two episodes of the Indosinian thermal event on the South China Block: constraints from LA-ICPMS U-Pb zircon and electron microprobe monazite ages of the Darongshan S-type granitic suite. Gondwana Res 19:1008–1023

Choukroune P (1992) Tectonic evolution of the Pyrenees. Annu Rev Earth Planet Sci 20:143–158

Chu Y (2012) Intracontinental tectonics in the South China block. Example of the Xuefengshan Belt. PhD Dissertation. Université d'Orléans

Chu Y, Faure M, Lin W, Wang QC (2011) Early Mesozoic intracontinental Xuefengshan Belt, South China: insights from structural analysis of polyphase deformation. EGU meeting, Vienna, Austria

Cocherie A, Albarede F (2001) An improved U-Th-Pb age calculation for electron microprobe dating of monazite. Geochim Cosmochim Acta 65:4509−4522

Deng XG, Chen ZG, Li XH (2004) SHRIMP U-Pb zircon dating of the Darongshan-Shiwandashan. Geol Rev 50:426–432

Dickinson WR, Snyder WS (1978) Plate tectonics of the Laramide orogeny. In: Matthews Ili V (ed) Laramide folding associated with Basement Block faulting in the Western United States. Geol Soc Am Mem 151:355–366

Ding X, Chen PR, Chen WF, Huang HY, Zhou XM (2005) LA-ICPMS zircon U-Pb age determination of the Weishan granite in Hunan: petrogenesis and significance. Sci China (D) 35: 606–616

Engebretson DC, Cox A, Gordon RG (1985) Relative motion between oceanic and continental plates in the Pacific basin. Geol Soc Am Special Pap 206:1–55

English JM, Johnston ST (2004) The Laramide orogeny: what were the driving forces? Int Geol Rev 46:833–838

Escher A, Beaumont C (1997) Formation, burial and exhumation of basement nappes at crustal scale: a geometric model based on the Western Swiss-Italian Alps. J Struct Geol 19:955–974

Faure M, Sun Y, Shu LS, Monié P, Charvet J (1996) Extensional tectonics within a subduction-type orogen. The case study of the Wugongshan dome (Jiangxi Province, southeastern China). Tectonophysics 263:77–106

Faure M, Lin W, Shu LS, Sun Y, Scharer U (1999) Tectonics of the Dabieshan (eastern China) and possible exhumation mechanism of ultra high-pressure rocks. Terra Nova 11:251–258

Faure M, Lin W, Monié P, Meffre S (2008) Paleozoic collision between the North and South China blocks, Early Triassic tectonics and the problem of the ultrahigh-pressure metamorphism. Comptes Rendus Geosci 340:139–150

Faure M, Shu LS, Wang B, Charvet J, Choulet F, Monie P (2009) Intracontinental subduction: a possible mechanism for the Early Palaeozoic Orogen of SE China. Terra Nova 21:360–368

Hacker BR, Wang QC (1995) Ar/Ar geochronology of ultrahigh-pressure metamorphism in Central China. Tectonics 14:994–1006

Hand M, Sandiford M (1999) Intraplate deformation in central Australia, the link between subsidence and fault reactivation. Tectonophysics 305:121–140

Harrowfield MJ, Wilson CJL (2005) Indosinian deformation of the Songpan Garze Fold Belt, northeast Tibetan Plateau. J Struct Geol 27:101–117

Haschke M, Siebel W, Gunther A, Scheuber E (2002) Repeated crustal thickening and recycling during the Andean orogeny in north Chile (21 degrees-26 degrees S). J Geophys Res 107(B1):2019. doi:10.1029/2001JB000328

Hendrix MS, Graham SA, Carroll AR, Sobel ER, McKnight CL, Schulein BJ, Wang Z (1992) Sedimentary record and climatic implications of recurrent deformation in the Tian Shan: evidence from Mesozoic strata of the north Tarim, south Junggar, and Turpan basins, northwest China. Geol Soc Am Bull 104:53–79

Holdsworth RE, Hand M, Miller JA, Buick IS (2001) Continental reactivation and reworking: an introduction. In: Miller JA, Holdsworth RE, Buick IS, Hand M (eds) Continental reactivation and reworking. Geological Society Publishing House, Bath, pp 1–12

Kusky TM, Ye M, Wang JP, Wang L (2010) Geological evolution of Longhushan World Geopark in relation to global tectonics. J Earth Sci 21:1–18

Lepvrier C, Maluski H, Van Vuong N, Roques D, Axente V, Rangin C (1997) Indosinian NW-trending shear zones within the Truong Son belt (Vietnam) ^{40}Ar-^{39}Ar Triassic ages and Cretaceous to Cenozoic overprints. Tectonophysics 283:105–127

Lepvrier C, Maluski H, Van Tich V, Leyreloup A, Truong Thi P, Van Vuong N (2004) The Early Triassic Indosinian orogeny in Vietnam (Truong Son Belt and Kontum Massif); implications for the geodynamic evolution of Indochina. Tectonophysics 393:87–118

Lepvrier C, Van Vuong N, Maluski H, Truong Thi P, Van Vu T (2008) Indosinian tectonics in Vietnam. Comptes Rendus Geosci 340:94–111

Lepvrier C, Faure M, Van VN, Vu TV, Lin W, Trong TT, Hoa PT (2011) North-directed Triassic nappes in Northeastern Vietnam (East Bac Bo). J Asian Earth Sci 41:56–68

Li XH (1999) U-Pb zircon ages of granites from the southern margin of the Yangtze Block: timing of Neoproterozoic Jinning: orogeny in SE China and implications for Rodinia Assembly. Precambrian Res 97:43–57

Li ZX, Li XH (2007) Formation of the 1300-km-wide intracontinental orogen and postorogenic magmatic province in Mesozoic South China: a flat-slab subduction model. Geology 35:179–182

Li XH, Li ZX, Li WX, Wang YJ (2006) Initiation of the Indosinian orogeny in South China: evidence for a Permian magmatic arc on Hainan Island. The J Geol 114:341–353

Li HQ, Wang DH, Chen FW, Mei YP, Cai H (2008) Study on chronology of the Chanziping and Daping gold deposit in Xuefeng Mountains,Hunan Province. Acta Geol Sinica 82:900–905 (in Chinese with English abstract)

Li XH, Li WX, Li ZX, Lo CH, Wang J, Ye MF, Yang YH (2009) Amalgamation between the Yangtze and Cathaysia Blocks in South China: Constraints from SHRIMP U-Pb zircon ages, geochemistry and Nd-Hf isotopes of the Shuangxiwu volcanic rocks. Precambrian Res 174:117–128

Li QL, Li XH, Liu Y, Tang GQ, Yang JH, Zhu WG (2010a) Precise U-Pb and Pb–Pb dating of Phanerozoic baddeleyite by SIMS with oxygen flooding technique. J Anal Atom Spectrom 25:1107–1113

Li ZX, Li XH, Wartho JA, Clark C, Li WX, Zhang CL, Bao C (2010b) Magmatic and metamorphic events during the early Paleozoic Wuyi-Yunkai orogeny, southeastern South China: new age constraints and pressure-temperature conditions. Geol Soc Am Bull 122:772–793

Lin W, Wang QC, Chen K (2008) Phanerozoic tectonics of south China block: new insights from the polyphase deformation in the Yunkai massif. Tectonics 27:TC6004. doi:10.1029/2007TC002207

Mattauer M, Matte P, Malavieille J, Tapponnier P, Maluski H, Xu ZQ, Lu YL, Tang YQ (1985) Tectonics of the Qinling Belt—buildup and evolution of Eastern Asia. Nature 317:496–500

McQuarrie N (2004) Crustal scale geometry of the Zagros fold-thrust belt, Iran. J Struct Geol 26:519–535

Molnar P, Tapponnier P (1975) Cenozoic tectonics of Asia: effects of a continental collision: features of recent continental tectonics in Asia can be interpreted as results of the India-Eurasia collision. Science 189:419–426

Passchier CW, Trouw RAJ (2005) Microtectonics, 2nd edn. Springer, Berlin, pp 27–66

Qiu YX, Zhang YC, Ma WP (1998) Tectonics and geological evolution of Xuefeng intra-continental orogene, South China. Geol J China Univ 4:432–443 (in Chinese with English abstract)

Qiu YX, Zhang YC, Ma WP (1999) The tectonic nature and evolution of Xuefeng Mountains: one model of formation and evolution of intra-continental Orogenic Belt. Geological Publishing House, Beijing

Raimondo T, Collins AS, Hand M, Walker-Hallam A, Smithies RH, Evins PM, Howard HM (2010) The anatomy of a deep intracontinental orogen. Tectonics 29:TC4024. doi:10.1029/2009tc002504

Roger F, Jolivet M, Malavieille J (2008) Tectonic evolution of the Triassic fold belts of Tibet. Comptes Rendus Geosci 340:180–189

Roger F, Jolivet M, Malavieille J (2010) The tectonic evolution of the Songpan-Garze (North Tibet) and adjacent areas from Proterozoic to present: a synthesis. J Asian Earth Sci 39:254–269

Roure F, Choukroune P, Berastegui X, Munoz JA, Villien A, Matheron P, Bareyt M, Seguret M, Camara P, Deramond J (1989) ECORS Deep seismic data and balanced cross sections: geometric constraints on the evolution of the Pyrenees. Tectonics 8:41–50

Sandiford M, Hand M, McLaren S (2001) Tectonic feedback, intraplate orogeny and the geochemical structure of the crust: a central Australian perspective. Geol Soc Lond Special Publ 184:195–218

Sibuet JC, Srivastava SP, Spakman W (2004) Pyrenean orogeny and plate kinematics. J Geophys Res 109. doi:10.1029/2003JB002514

Stipp M, Stuitz H, Heilbronner R, Schmid SM (2002) The eastern Tonale fault zone: a 'natural laboratory' for crystal plastic deformation of quartz over a temperature range from 250 to 700°C. J Struct Geol 24:1861–1884

Suzuki K, Adachi M (1991) Precambrian provenance and Silurian metamorphism of the Tsubonosawa paragneiss in the south Kitakami terrane, northeast Japan, revealed by the chemical Th-U-total Pb isochron ages of monazite, zircon and xenotime. Geochem J 25:357–376

Tapponnier P, Molnar P (1979) Active faulting and Cenozoic tectonics of the Tienshan, Mongolia, and Baykal regions. J Geophys Res 84:3425–3459

Tullis J, Christie JM, Griggs DT (1973) Microstructures and preferred orientations of experimentally deformed quartzites. Geol Soc Am Bull 84:297–314

Wallis S, Tsujimori T, Aoya M, Kawakami T, Terada K, Suzuki K, Hyodo H (2003) Cenozoic and Mesozoic metamorphism in the Longmenshan orogens: implications for geodynamic models of eastern Tibet. Geology 31:745–748

Wan YS, Liu DY, Wilde SA, Cao J, Chen B, Dong C, Song B, Du L (2009) Evolution of the Yunkai Terrane, South China: evidence from SHRIMP zircon U-Pb dating, geochemistry and Nd isotope. J Asian Earth Sci 37:140–153

Wang J, Li ZX (2003) History of Neoproterozoic rift basins in South China: implications for Rodinia break-up. Precambrian Res 122:141–158

Wang XF, Metcalfe I, Jian P, He LQ, Wang CS (2000) The Jinshajiang-Ailaoshan Suture Zone, China: tectonostratigraphy, age and evolution. J Asian Earth Sci 18:675–690

Wang YJ, Fan WM, Guo F, Peng TP, Li CW (2003) Geochemistry of Mesozoic mafic rocks adjacent to the Chenzhou-Linwu fault, South China: implications for the lithospheric boundary between the Yangtze and Cathaysia blocks. Int Geol Rev 45(3):263–286

Wang YJ, Zhang YH, Fan WM, Peng TP (2005) Structural signatures and Ar-40/Ar-39 geochronology of the Indosinian Xuefengshan tectonic belt, South China Block. J Struct Geol 27:985–998

Wang YJ, Fan WM, Sun M, Liang XQ, Zhang YH, Peng TP (2007a) Geochronological, geochemical and geothermal constraints on petrogenesis of the Indosinian peraluminous granites in the South China Block: a case study in the Hunan Province. Lithos 96:475–502

Wang YJ, Fan WM, Zhao GC, Ji SC, Peng TP (2007b) Zircon U-Pb geochronology of gneissic rocks in the Yunkai massif and its implications on the Caledonian event in the South China Block. Gondwana Res 12:404–416

Xiao WJ, He HQ (2005) Early Mesozoic thrust tectonics of the northwest Zhejiang region (Southeast China). Geol Soc Am Bull 117:945–961

Xu HJ, Ma CQ, Zhong YF, She ZB (2004) Zircon SHRIMP dating of Taojiang and Dashenshan granite: lower limit on the timing of the amalgamation between Yangtze and Cathaysia blocks. Annual Meeting of Petrology and Geodynamics, China

Xu XB, Zhang YQ, Shu LS, Jia D (2011) La-ICP-MS U-Pb and 40Ar/39Ar geochronology of the sheared metamorphic rocks in the Wuyishan: constraints on the timing of Early Paleozoic and Early Mesozoic tectono-thermal events in SE China. Tectonophysics 501:71–86

Yan DP, Zhou MF, Song HL, Wang XW, Malpas J (2003) Origin and tectonic significance of a Mesozoic multi-layer over-thrust system within the Yangtze Block (South China). Tectonophysics 361:239–254

Zhang Z, Wang Y (2007) Crustal structure and contact relationship revealed from deep seismic sounding data in South China. Phys Earth Planet Inter 165(1–2):114–126

Zhou XM (2007) Genesis of Late Mesozoic granites in Nanling region and geodynamic evolution of lithosphere. Science Press, Beijing, pp 1–691